Inorg. Chem. **2008**, *47*, 7493−7511

Effects of Excited State−Excited State Configurational Mixing on Emission Bandshape Variations in Ruthenium−Bipyridine Complexes

Onduru S. Odongo,[†] Mary Jane Heeg,[†] Yuan-Jang Chen,[‡] Puhui Xie,[†] and John F. Endicott*,[†]

Department of Chemistry, Wayne State University, Detroit, Michigan 48202, and Department of Chemistry, Fu Jen Catholic University, Taipei Hsien 24205, Taiwan, R.O.C.

Received December 18, 2007

The 77 K emission spectra of 21 $[Ru(L)_4bpy]^{m+}$ complexes for which the Ru/bpy metal-to-ligand-charge-transfer (^{3}MLCT) excited-state energies vary from 12 500 to 18 500 cm^{-1} have vibronic contributions to their bandshapes that implicate excited-state distortions in low frequency (*lf*; $h\nu_{lf}$ < 1000 cm^{-1}), largely metal−ligand vibrational modes which most likely result from configurational mixing between the ^{3}MLCT and a higher energy metal centered (^{3}LF) excited state. The amplitudes of the *lf* vibronic contributions are often comparable to, or sometimes greater than those of medium frequency (*mf*; $h\nu_{mf}$ > 1000 cm^{-1}), largely bipyridine (bpy) vibrational modes, and for the $[Ru(bpy)_3]^{2+}$ and $[Ru(NH_3)_4bpy]^{2+}$ complexes they are consistent with previously reported resonance-Raman (rR) parameters. However, far smaller *lf* vibronic amplitudes in the rR parameters have been reported for $[Os(bpy)_3]^{2+}$, and this leads to a group frequency approach for interpreting the 77 K emission bandshapes of $[Ru(L)_4bpy]^{m+}$ complexes with the vibronic contributions from *mf* vibrational modes referenced to the $[Os(bpy)_3]^{2+}$ rR parameters (OB3 model) and the envelope of *lf* vibronic components represented by a "progression" in an "equivalent" single vibrational mode (*lf*1 model). The *lf*1 model is referenced to rR parameters reported for $[Ru(NH_3)_4bpy]^{2+}$. The observation of *lf* vibronic components indicates that the MLCT excited-state potential energy surfaces of Ru-bpy complexes are distorted by LF/MLCT excited-state/excited-state configurational mixing, but the emission spectra only probe the region near the ^{3}MLCT potential energy minimum, and the mixing can lead to larger distortions elsewhere with potential photochemical implications: (a) such distortions may labilize the ^{3}MLCT excited state; and (b) the *lf* vibrational modes may contribute to a temperature dependent pathway for nonradiative relaxation.

Introduction

The potential of ruthenium(II)-polypyridyl based "dyes" to function as mediators for the conversion of solar to electrical or chemical energy has received considerable attention.[1−11] To a large extent this potential arises because some electronic excited states of transition metal complexes are facile electron transfer agents that can be generated by visible light absorption.[1,2,6] While it has long been established that electron transfer reactivity depends on the accompanying changes in molecular structure,[12−21] there are few experimental measures of the structures of electronic excited states and, with notable exceptions,[11] their treatment is often based

* To whom correspondence should be addressed. E-mail: jfe@chem.wayne.edu.
† Wayne State University.
‡ Fu Jen Catholic University.

(1) Gratzel, M. *Inorg. Chem.* **2005**, *44*, 6841.
(2) Gratzel, M.; Moser, J.-E. In *Electron Transfer in Chemistry*; Balzani, V. , Ed.; Wiley-VCH:Weinheim, 2001; Vol. *5*; p 589.
(3) Gust, D.; Moore, T. A.; Moore, A. L. *Acc. Chem. Res.* **2001**, *34*, 40.
(4) Hagfeldt, A.; Gratzel, M. *Acc. Chem. Res.* **2000**, *33*, 269.
(5) Hahn, U.; Gorka, M.; Vogtle, F.; Vicinelli, V.; Ceroni, P.; Maestri, M.; Balzani, V. *Angew. Chem., Int. Ed.* **2002**, *41*, 3595.
(6) Meyer, G. J. *Inorg. Chem.* **2005**, *44*, 6802.
(7) Schwartzburg, K.; Ernstorfer, R.; Felber, S.; Willig, F. *Coord. Chem. Rev.* **2004**, *248*, 1259.
(8) Asbury, J. B.; Ellingson, R. J.; Ghosh, H. N.; Ferrere, S.; Nozik, A. J.; Lian, T. Q. *J. Phys. Chem. B* **1999**, *103*, 3110.
(9) Barolo, C.; Nazeeruddin, M. K.; Fantacci, S.; Di Censo, D.; Comte, P.; Liska, P.; Vicardi, G.; Quagliotto, P.; De Angelis, F.; Ito, S.; Graetzel, M. *Inorg. Chem.* **2006**, *45*, 4642.
(10) Creutz, C.; Brunschwig, B. S.; Sutin, N. *J. Phys. Chem. B* **2006**, *110*, 25181.
(11) Staniszewski, A.; Morris, A. J.; Ito, T.; Meyer, G. J. *J. Phys. Chem. B* **2007**, *111*, 6822.
(12) Taube, H. *Can. J. Chem.* **1959**, *37*, 129.
(13) Marcus, R. A. *Discuss. Faraday Soc.* **1960**, *29*, 21.
(14) Marcus, R. A. *Annu. Rev. Phys. Chem.* **1964**, *15*, 155.
(15) Hush, N. S. *Prog. Inorg. Chem.* **1967**, *8*, 391.
(16) Cannon, R. D. *Electron Transfer Reactions*; Butterworth: London, 1980.
(17) Sutin, N. *Prog. Inorg. Chem.* **1983**, *30*, 441.
(18) Newton, M. D.; Sutin, N. *Annu. Rev. Phys. Chem.* **1984**, *35*, 437.

10.1021/ic7024473 CCC: $40.75
Published on Web 08/06/2008

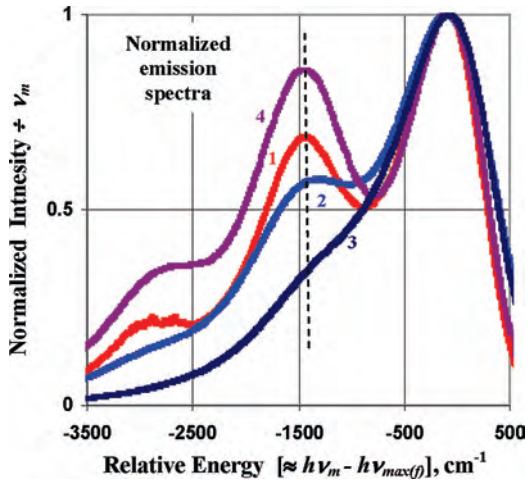

Figure 1. Superimposed 77 K emission spectra of $[Ru(bpy)_3]^{2+}$ (1),[26] $[Ru(NH_3)_4bpy]^{2+}$ (2),[26] $[Ru([12]aneN_4))bpy]^{2+}$ (3),[27] and $[Ru(CH_3CN)_2(bpy)_2]^{2+}$ (4). To facilitate the comparisons, the intensity scale is defined so that $I_{max(em)} = 1.00$ for the highest energy component and the abscissa is chosen so that maxima of these components of the different spectra coincide. This energy scale approximately corresponds to the difference between the observed emission energy and the energy maximum of the fundamental component[37] ($\approx -h\nu_d$, below). Note that $h\nu_{max(f)}$ varies from 12 500 to 18 500 cm^{-1} and ($h\nu_{max(f)} - h\nu_{max(emis)}$) from 90 to 260 cm^{-1} for the different complexes (see Table 2). The approximate maximum energy expected for the envelope of contributions from distortions in bpy vibrational modes ($h\nu_d \sim 1440$ cm^{-1}) is indicated by the vertical dashed line.

on analogy with ground-state species. Such analogies are bound to be misleading since excited-state electronic configurations tend to be unique and since heavy metal complexes typically have many near-in-energy excited states with the potential for configurational mixing which can modify the molecular structure of the lowest energy excited state, and thereby, its electron transfer reactivity. Because the vibronic contributions to emission bandshapes are functions of the differences in ground-state and excited-state molecular structures,[22–25] the excited-state structural variations that result from configurational mixing will be manifested in correlated variations in emission bandshapes.

A very wide range of emission bandshapes has been found for the metal-to-ligand charge transfer (MLCT) excited states of simple Ru/bpy complexes in frozen solutions (e.g., see Figure 1),[26–28] and this indicates that there are appreciable variations in the corresponding ^{3}MLCT excited-state molecular structures. The dominant features of most 77 K Ru-bpy emission spectra are often attributed to the following:[29–36] (a) the intensity of the $\{e,0'\} \rightarrow \{g,0\}$ emission component; and (b) distortions in bpy-centered vibrational modes (or a single "equivalent" mode)[29–31,34–36] which give rise to a sideband component whose dominant feature is usually observed at 1300−1500 cm^{-1} lower energy than that of the $\{e,0'\}\rightarrow\{g,0\}$ component.

Careful examination of the 77 K emission spectra of this class of complexes indicates that such simple interpretations of the emission bandshapes are incorrect.[37] Thus, even in Figure 1 the spectra demonstrate the following: that (a) the MLCT excited-state distortions vary over a very large range in very closely related complexes; and (b) the simple model that such distortions occur in only bpy vibrational modes is not always correct. The complexity of the vibronic sideband contributions is demonstrated more clearly in Figure 2 in which the contributions of the best fit fundamental components, $I_{\nu_m(f)}$ (deconvoluted from the observed spectra),[26,37–39] have been removed from the emission spectra (I_{ν_m}) of Figure 1 to generate a difference spectrum, $A_{\nu_m(diff)}$,

$$A_{\nu_m(diff)} = \frac{I_{\nu_m} - I_{\nu_m(f)}}{I_{max(f)}} \qquad (1)$$

The difference spectra in Figure 2 demonstrate that even such weakly structured spectra as those of Figure 1 contain

(19) Meyer, T. J.; Taube, H. In *Comprehensive Coordination Chemistry*; Wilkinson, G., Gillard, R. D., McCleverty, J., Eds.; Pergamon: Oxford, England, 1987; Vol. *7*; p 331.
(20) Sutin, N. *Adv. Chem. Phys.* **1999**, *106*, 7.
(21) Endicott, J. F. In *Comprehensive Coordination Chemistry II*, 2nd ed.; McCleverty, J., Meyer, T. J., Eds.; Pergamon:Oxford, U.K., 2003; Vol. *7*, p 657.
(22) Solomon, E. I. *Comments Inorg. Chem.* **1984**, *3*, 225.
(23) Gould, I. R.; Noukakis, D.; Gomez-Jahn, L.; Young, R. H.; Goodman, J. L.; Farid, S. *Chem. Phys.* **1993**, *176*, 439.
(24) Myers, A. B. *Chem. Phys.* **1994**, *180*, 215.
(25) Brunold, T. C.; Gudel, H. U. In *Inorganic Electronic Structure and Spectroscopy*; Solomon, E. I., Lever, A. B. P., Eds.; Wiley-Interscience: New York, 1999; Vol. *1*, p 259.
(26) Xie, P.; Chen, Y.-J.; Uddin, M. J.; Endicott, J. F. *J. Phys. Chem. A* **2005**, *109*, 4671.
(27) Chen, Y.-J.; Xie, P.; Heeg, M. J.; Endicott, J. F. *Inorg. Chem.* **2006**, *45*, 6282.
(28) Chen, Y.-J.; Xie, P.; Endicott, J. F.; Odongo, O. S. *J. Phys. Chem. A* **2006**, *110*, 7970.
(29) Casper, J. V.; Kober, E. M.; Sullivan, B. P.; Meyer, T. J. *J. Am. Chem. Soc.* **1982**, *104*, 630.
(30) Curtis, J. C.; Sullivan, B. P.; Meyer, T. J. *Inorg. Chem.* **1983**, *22*, 224.
(31) Kober, E. M.; Meyer, T. J. *Inorg. Chem.* **1985**, *24*, 106.
(32) Kober, E. M.; Casper, J. V.; Lumpkin, R. S.; Meyer, T. J. *J. Phys. Chem.* **1986**, *90*, 3722.
(33) Barbara, P. F.; Meyer, T. J.; Ratner, M. *J. Phys. Chem.* **1996**, *100*, 13148.
(34) Graff, D.; Claude, J. P.; Meyer, T. J. In *Electron Transfer Reactions: Inorganic, Organometallic and Biological Applications*; Isied, S. S., Ed.; American Chemical Society: Washington, DC, 1997; p 183.
(35) Thompson, D. W.; Fleming, C. N.; Myron, B. D.; Meyer, T. J. *J. Phys. Chem. B* **2007**, *111*, 6930.
(36) Thompson, D. G.; Schoonover, J. R.; Timpson, C. J.; Meyer, T. J. *J. Phys. Chem. A* **2003**, *107*, 10250.
(37) We have deconvoluted a best fit high energy component, $I_{\nu_m(f)}$, from the emission spectra as described previously[26] and in the Experimental Section. Under ideal circumstances this fundamental component is a good approximation of the emission component corresponding to the band origin, $I_{\nu_m(0'0)}$, but it is not a direct measurement of that component. To emphasize this distinction between $I_{\nu_m(f)}$ and the theoretical band origin component, we have referred to the former as the "fundamental component" of the emission spectrum.[26] This "fundamental component" is not to be confused with the first order term of a vibrational progression (usually called the "fundamental" in vibrational spectroscopy) which we refer to as the 1st order term. Our treatment leads to good to excellent fits of the published rR parameters to the experimental emission spectra as reported previously[1] and even to the reasonable, more detailed fits of the difference spectra as illustrated in Figures 6 and 7. $I_{max(0'0)}$ should contain a factor ϕ which is a function of the excited-state displacements.[38] Thus, for a single mode representation of the vibronic sideband $\phi = e^{-S_k}$ and the emission spectrum can be expressed as $I_{\nu_m(emis)} = (I_{max(0'0)}{}^o e^{-S_1}G_{0'0} + S_1 e^{-S_1}G_1 + S_1^2 e^{-S_1}G_{1+1} + .)$ where the G_x are appropriate Gaussian bandshape functions. Then, for $(I_{max(0'0)}{}^o e^{-S_1}G_{0'0}) \approx I_{\nu_m(f)}$, the normalized difference spectrum is $(I_{\nu_m(emis)} - I_{\nu_m(f)})/I_{max(f)} = [(S_1 e^{-S_1}G_1)/I_{max(f)}] + . .$ and the maximum possible normalized ($I_{max(f)} = 1$) sideband amplitude is $e^{-1} = 0.378$. The maximum difference spectrum amplitudes of the Ru-bpy complexes that we have examined are greater than 0.4.
(38) Myers, A. B.; Mathies, R. A.; Tannor, D. J.; Heller, E. J. *J. Chem. Phys.* **1982**, *77*, 3587.
(39) Supporting Information, see the paragraph at the end of this paper.

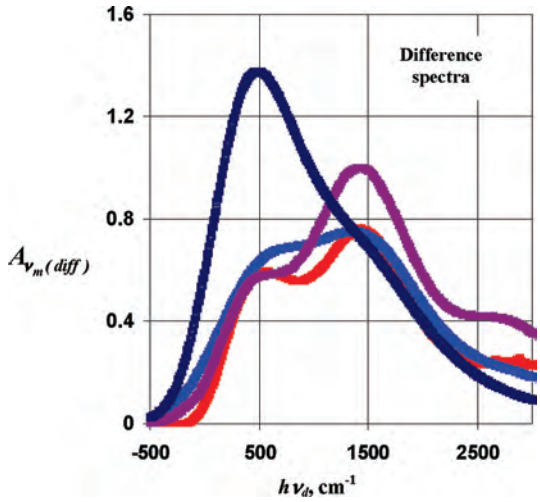

Figure 2. Comparisons of vibronic contributions to 77 K emission bandshapes ($A_{\nu_m(diff)}$) for $[Ru(bpy)_3]^{2+}$ (red), $[Ru(NH_3)_4bpy]^{2+}$ (blue), and $[Ru(CH_3CN)_2(bpy)_2]^{2+}$ (dark red) and $[Ru([12]aneN_4))bpy]^{2+}$ (dark blue). The ordinate is based on eq 1 and $h\nu_d = (h\nu_{max(f)} - h\nu_{m(em)})$.

significant vibronic information: (a) the sideband amplitudes are all greater than the simple theoretical limit for distortions only in a single bpy vibrational mode;[37] and (b) each of these emission spectra has a strong, or dominant in the case of $[Ru([12]aneN_4)bpy]^{2+}$, vibronic feature near $(h\nu_{max(f)} - h\nu_{m(em)}) = h\nu_d = 500$ cm^{-1}. Further to this point, significant low frequency (*lf*; hν_d < 1000 cm^{-1}) vibronic components have been reported in the resonance-Raman (rR) spectra of $[Ru(bpy)_3]^{2+}$[40] and $[Ru(NH_3)_4bpy]^{2+}$.[41] Such vibronic features are consistent with distortions in metal−ligand vibrational modes, and their variations in amplitude are very likely to be the result of differences in the extents of excited-state/excited-state configurational mixing through this series of complexes.

The rR parameters reported for $[Ru(bpy)_3]^{2+}$,[40] $[Ru(NH_3)_4bpy]^{2+}$,[41] and $[Os(bpy)_3]^{2+}$[36] (see Supporting Information, Table S1)[39] indicate that there are distortions in a dozen or more vibrational modes of their MLCT excited states. Therefore, the shapes of the emission sidebands in broadband spectra should be attributed to the overlapping contributions of individual distortion modes, and the rR parameters reported for the $[Ru(bpy)_3]^{2+}$ and $[Ru(NH_3)_4bpy]^{2+}$ complexes give good to excellent fits of the observed bandshapes when the amplitude scale (as in eq 1) and the component bandwidths are those determined by their experimental fundamental components.[26] Furthermore, the observed spectral sideband contributions, such as noted in Figure 2, and rR-based modeling[26] suggest that the emission sideband envelopes of these complexes can be approximately separated into significant component vibronic envelopes that arise from distortions in the following: (a) the several vibrational modes that are largely associated with the bpy ligand, $I_{\nu_m(bpy)}$;[42] and (b) the *lf* vibronic components that are largely associated with metal−ligand vibrational modes, $I_{\nu_m(ML)}$. That these vibronic components are approximately independent is suggested by the similar amplitudes of the $I_{\nu_m(bpy)}$ components based on the respective rR parameters for the $[Ru(bpy)_3]^{2+}$ and $[Os(bpy)_3]^{2+}$ complexes, but much

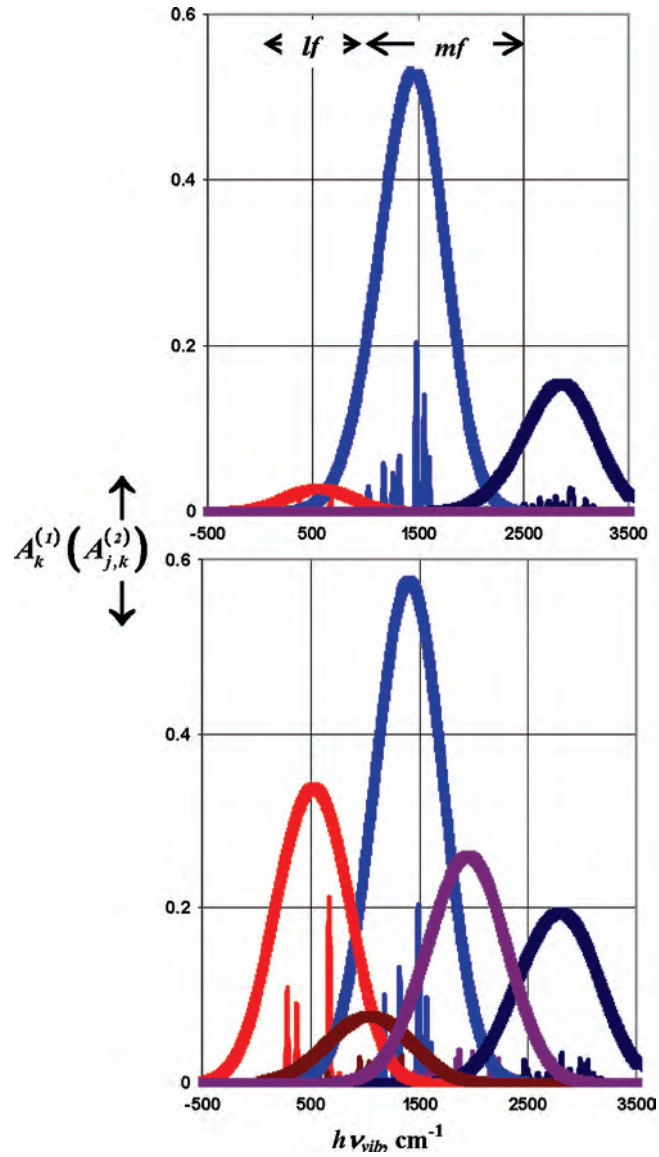

Figure 3. Envelopes calculated for the 1st and 2nd order vibronic contributions based on rR parameters for $[Os(bpy)_3]^{2+}$,[36] upper panel; and $[Ru(bpy)_3]^{2+}$,[40] lower panel. The first order contributions are indicated in red for the *lf* regime ($h\nu_{vib}$ < 1000 cm^{-1}; ν_{vib} = the frequency difference from the electronic band origin) and blue for the *mf* regime (1000 < $h\nu_{vib}$/cm^{-1} < 2000); the 2nd order contributions are indicated in dark red for $\nu_{vib} = (\nu_j + \nu_k)$ with ν_j, ν_k < 1000 cm^{-1}, in dark blue for 1000 < ($h\nu_j$, $h\nu_k$/cm^{-1}) < 2000, and in violet for all ν_{vib} for which ν_j < 1000 cm^{-1} and ν_k > 1000 cm^{-1} (*lf*, *mf* combination bands). The first order envelopes were calculated from rR parameters (ν_j, ν_k, S_j, and S_k) as $A^{(1)} = \sum_k S_k e^{-S_k} e^{-(\nu_k - \nu_{vib})^2/w^2}$ where $S_k = \lambda_k/h\nu_k$, λ_k is the vibrational reorganizational energy for the *k*th first order mode (proportional to the squared displacement in that mode), $w = (\Delta\nu_{1/2})/(4 \ln 2)$ and $\Delta\nu_{1/2}$ = 620 cm^{-1}; the 2nd order envelopes were calculated as $A^{(2)} = \sum_j \sum_k e^{-(S_j+S_k)/2} e^{-(\nu_{vib}-\nu_j-\nu_k)^2/w^2}$. The narrow lines, calculated (with $\Delta\nu_{1/2}$ = 20 cm^{-1}) and color coded as above, illustrate the amplitudes of the S_ν parameters for the first order terms; note that all of the 2nd order terms with $\Delta\nu_{1/2}$ = 20 cm^{-1} are present in this figure but their amplitudes are often too small to be seen on the scale used (see also Supporting Information, Figure S7).[39] Note that the larger amplitudes of the envelopes calculated with $\Delta\nu_{1/2}$ = 620 cm^{-1} arise only from the overlapping contributions of the individual vibronic components.

(40) Maruszewski, K.; Bajdor, K.; Strommen, D. P.; Kincaid, J. R. *J. Phys. Chem.* **1995**, *99*, 6286.
(41) Hupp, J. T.; Williams, R. T. *Acc. Chem. Res.* **2001**, *34*, 808.
(42) Stromen, D. P.; Mallick, P. K.; Danzer, G. D.; Lumpkin, R. S.; Kincaid, J. R. *J. Phys. Chem.* **1990**, *94*, 1357.

smaller amplitudes of *lf* components for the latter,[36] as illustrated in Figure 3. This comparison suggests that the shapes of the $I_{\nu_m(bpy)}$ contributions should be transferable from one complex to another.

In an idealized (diabatic) limit with no configurational mixing between excited states, a Ru/bpy MLCT excited state (with a $Ru^{III}(d\pi^5)$-bpy (π^*) electronic configuration) would be expected to be mostly distorted in bpy vibrational modes while a metal centered (or ligand field; LF) Ru^{II} excited state with a $d\pi^5 d\sigma^*$ electronic configuration would be distorted in relatively *lf* metal−ligand vibrational modes. The nonradiative relaxation of the MLCT excited state in this limit corresponds to a simple electron transfer process and can be compared to the well characterized Ru(III)/Ru(II) self-exchange electron transfer processes in solution[19,21] which involve a change of electron density in the largely nonbonding $d\pi$ orbitals with little corresponding change in molecular structure.[19,21] The nearly negligible Ru-ligand reorganizational energy contributions associated with this electron transfer process are inconsistent with the appreciable *lf* vibronic contributions evident in the rR[40,41] and emission spectra[26–28] of the $[Ru(L)_4bpy]^{2+}$ complexes (Figures 2 and 3).[43,44] On the other hand, the $d\pi^5 d\sigma^*$ excited states of nd^6 metals are very highly distorted,[45,46] so that configurational mixing of a ^{3}MLCT excited state with a higher energy ^{3}LF excited state can greatly increase the metal−ligand distortions of the former and the amplitudes of *lf* vibronic contributions to the emission sideband and thereby account for their relatively large $I_{\nu_m(ML)}$ amplitudes. Consequently, the variations in emission bandshapes of the MLCT excited states of simple $[Ru(L)_4bpy]^{m+}$ complexes may be attributable to variations in the extents of configurational mixing among their electronic states.[26–28,43,44,47–51]

The above considerations suggest that it may be possible to approximately resolve the 77 K emission spectra of Ru-bpy complexes into contributions that arise from identifiable functional groups within the complex so that

$$I_{\nu_m} \cong I_{\nu_m(f)} + I_{\nu_m(bpy)} + I_{\nu_m(ML)} + I_{\nu_m(OT)} \qquad (2)$$

Each of the terms in eq 2 that represents the vibronic contributions of different functional groups (e.g., with s = *ML* or *bpy*) is to be interpreted as the envelope of the sum of overlapping vibronic progressions (j = 1, 2,...) in all of the relevant molecular vibrational modes, k,

$$I_{\nu_m(s)} = \sum_k I_{\nu_m(k)} = \sum_k \left(\sum_j I_{\nu_m(0-j)} \right)_k \qquad (3)$$

The $I_{\nu_m(OT)}$ term contains spectral sideband contributions other than those that can be attributed to distortions in predominately bpy or metal−ligand vibrational modes, combination band contributions, and so forth. The systematic evaluation of molecular structure variations in a series of complexes depends on reliable approaches to modeling $I_{\nu_m(f)}$, $I_{\nu_m(bpy)}$, and $I_{\nu_m(ML)}$. We have elsewhere discussed systematic procedures for evaluating the contributions of the fundamental components, $I_{\nu_m(f)}$.[26,37,43,44] In this report we consider systematic approaches to the estimation of $I_{\nu_m(bpy)}$ and $I_{\nu_m(ML)}$ for a wide range of $[Ru(L)_4bpy]^{m+}$ complexes.

In addition to low energy MLCT and LF excited states, these complexes can also possess other types of excited states that are reasonably low in energy such as ligand-to-ligand charge transfer (LLCT) and internal ligand (IL; $\pi\pi^*$) excited states,[9,52–60] and variations in the configurational mixings with these states from complex-to-complex could also alter the emission bandshapes and electron transfer properties of the lowest energy MLCT excited states. Thus, a recent report has noted that the lowest energy excited states of some Ru-polypyridyl complexes which have features appropriate to good photosensitizers may have mixed MLCT, and LLCT character.[9] In principle, such "mixed character" of the lowest energy excited state could result in enhanced excited-state charge separation. More generally, configurational mixing between excited states will result in a lowest energy adiabatic excited state which is distorted along nuclear coordinates that in the diabatic limit are unique to the higher energy excited state (e.g., to $I_{\nu_m(ML)}$ or $I_{\nu_m(OT)}$ in eq 1). However, some of these distortions will correspond to vibronic components which overlap with those of the $I_{\nu_m(bpy)}$ or $I_{\nu_m(ML)}$ envelopes, so their identification is difficult and dependent on the evaluation of the dominant components in eq 2. A systematic approach for determining the $I_{\nu_m(ML)}$ and $I_{\nu_m(bpy)}$ vibronic contributions to MLCT emission sidebands is developed in this report and applied to several classes of simple $[Ru(L)_4bpy]^{m+}$ complexes.

Experimental Section

A. Materials. The synthesis properties of the $[Ru(L)_{6-2n}(bpy)_n]^{2+}$ complexes with $(L)_4$ = $(NH_3)_4$, (en = ethylenediamine)$_2$, trien (triethylenetetramine), [12]aneN$_4$ (1,4,7,10-tetraazacyclododecane), [14]aneN$_4$ (1,4,8,11-tetraazacyclotetradecane), and (py = pyridine)$_4$ are discussed elsewhere;[26–28] skeletal structures of the ligands are

(43) Endicott, J. F.; Chen, Y.-J. *Coord. Chem. Rev.* **2007**, *251*, 328.
(44) Endicott, J. F.; Chen, Y.-J.; Xie, P. *Coord. Chem. Rev.* **2005**, *249*, 343.
(45) Hakamata, K.; Urushiyama, A.; Kupka, H. *J. Phys. Chem.* **1981**, *85*, 1983.
(46) Wilson, R. B.; Solomon, E. I. *J. Am. Chem. Soc.* **1980**, *102*, 4085.
(47) Chen, Y.-J.; McNamara, P. G.; Endicott, J. F. *J. Phys. Chem.* **2007**, *111*, 6748.
(48) Xie, P.; Chen, Y.-J.; Endicott, J. F.; Uddin, M. J.; Seneviratne, D.; McNamara, P. G. *Inorg. Chem.* **2003**, *42*, 5040.
(49) Chen, Y.-J.; Xie, P.; Endicott, J. F. *J. Phys. Chem. A* **2004**, *108*, 5041.
(50) Chen, Y.-J.; Endicott, J. F.; Swayambunathan, V. *Chem. Phys.* **2006**, *326*, 79.
(51) Endicott, J. F.; Chen, Y.-J. *Inorg. Chim. Acta* **2007**, *360*, 913.
(52) Stor, G. J.; Stufkens, D. J.; Oskam, A. *Inorg. Chem.* **1992**, *31*, 1318.
(53) Kimachi, S.; Ikeda, S.; Miki, H.; Azumi, T.; Crosby, G. A. *Coord. Chem. Rev.* **1994**, *132*, 43.
(54) Nazeeruddin, M. K.; Humphry-Baker, R.; Comte, P.; Liska, P.; Cevey, L.; Costa, E.; Shklover, V.; Spiccia, L.; Deacon, G. B.; Bignozzi, C. A.; Graetzel, M. *J. Am. Chem. Soc.* **2001**, *123*, 1613.
(55) Acosta, A.; Zink, J. I.; Cheon, J. *Inorg. Chem.* **2000**, *39*, 427.
(56) Vogler, A.; Kunkely, H. *Coord. Chem. Rev.* **2005**, *249*, 1511.
(57) Li, S.-W.; Cheng, Y.-M.; Yeh, Y.-S.; Hsu, C.-C.; Chou, P.-T.; Peng, S.-M.; Lee, G.-H.; Tung, Y.-L.; Wu, P.-C.; Chi, Y.; Wu, F.-I.; Shu, C.-F. *Chem.−Eur. J.* **2005**, *11*, 6347.
(58) Nazeeruddin, M. K.; Wang, Q.; Cevey, L.; Aranyos, V.; Liska, P.; Figgemeier, E.; Klein, F.; Hirata, N.; Koops, S.; Haque, S. A.; Durrant, J. R.; Hagfeldt, A.; Lever, A. B. P.; Graetzel, M. *Inorg. Chem.* **2006**, *455*, 787.
(59) Kunkely, H.; Vogler, A. *Inorg. Chim. Acta* **2006**, *359*, 388.
(60) Zhao, Q.; Liu, S.; Shi, M.; Wang, C.; Yu, M.; Li, L.; Li, F.; Yi, T.; Huang, C. *Inorg. Chem.* **2006**, *45*, 6152.

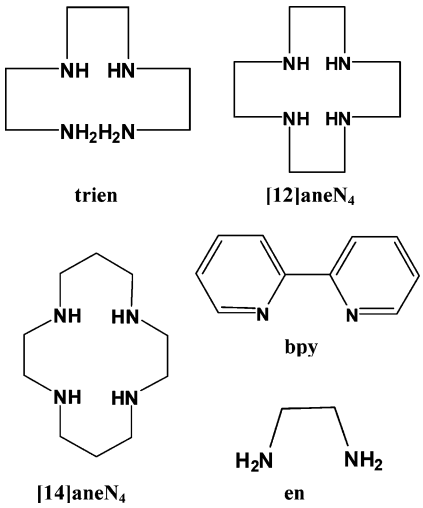

Figure 4. Skeletal structures of some of the ligands and abbreviations used in this article: trien = triethylenetetraamine; [12]aneN$_4$ = 1,4,7,10-tetraazacyclododecane; [14]aneN$_4$ = 1,4,8,11-tetraazacyclotetradecane; bpy = 2,2′-bipyridine; en = 1,2-diaminoethane.

shown in Figure 4. The syntheses, purification, and characterization of the $[Ru(CH_3CN)_n(X)_{2-n}(bpy)_2]^{n+}$, (X = Cl, Br, CN, NO_2, SCN; $(X)_2 = CO_3$, C_2O_4 and $C_3H_2O_4$) and $[Ru(py)_2(bpy)_2]^{2+}$ complexes employed variations of standard procedures;[61–64] these details are presented in the Supporting Information (S3).[39]

We have found the emission band shape of bis(acetonitrile)bis(2,2′-bipyridine)ruthenium, $[Ru(CH_3CN)_2(bpy)_2](PF_6)_2$, to be exceptionally sensitive to small amounts of impurities. Consequently we have used different approaches for the synthesis and purification of the preparative intermediates as well as the reaction products. The details are summarized in the Supporting Information.[39]

Acetonitrile-chloro-bis(2,2′-bipyridine)ruthenium Trifluoromethylsulfonate, [Ru (CH$_3$CN)(Cl)(bpy)$_2$]CF$_3$SO$_3$. A 0.2 g aliquot of $[Ru(bpy)_2Cl_2]$ complex suspended in 40 mL of acetonitrile was heated at 70 C for 1 h. The resulting solution was cooled to room temperature (rt) and combined with 40 mL of methanol. Reaction progress was followed by growth of the product absorption band at about 470 nm. Solvent was removed from the reaction mixture by rotary evaporation, and the crude product was loaded onto a neutral alumina column. The complex was purified using neutral alumina column chromatography with a methylene chloride:toluene: methanol eluant (50:50:1 v/v/v). Evaporation of solvent from the effluent provided X-ray quality orange-red crystals. ^{1}H NMR (400 MHz, methanol-d$_4$): δ 9.95 (d, 1H), 9.55 (d, 1H), 8.74 (d, 1H), 8.68 (d, 1H), 8.59 (dd, 2H), 8.30 (t,1H), 8.21 (t, 1H), 7.93 (m, 5H), 7.69 (d, 1H), 7.29 (m, 2H) (aromatic protons), 2.46 (CH3CN). ^{13}C NMR (400 MHz, methanol-d$_4$): δ 159.7, 158.9, 158.3, 158.0, 153.3 (2C), 152.9, 151.7, 137.4, 136.7, 136.5, 136.3, 126.9, 126.8, 126.5, 126.1, 123.6, 123.5 (2C), 123.2, 94.5, 2.6.

B. X-ray Structure Determination. Diffraction data were measured on a Bruker X8 APEX-II kappa geometry diffractometer[65] with Mo radiation and a graphite monochromator at 100 K. Frames were collected for 10 s with the detector at 40 mm and 0.3 degrees between each frame. Sheldrick's SHELX-97[66] software was used in the refinement and reporting of the model. Crystals appeared as red plates, and a sample approximately 0.3 × 0.16 × 0.02 mm^3 was used for data collection. 3498 frames were collected, yielding 50260 reflections, of which 6536 were independent. Hydrogen positions were placed in calculated positions. The asymmetric unit contains one cationic complex and one anion. A summary of the crystallographic parameters is given in Table 1, and further details can be found in the Supporting Information, S4.[39] The two bpy ligands are positioned cis and inclined at 86.27(4) deg. The acetonitrile is nearly linear at 178.6(3) deg. The Ru−N(bpy) bond distances are longer trans to bpy (2.054 Å avg.) and shorter trans to Cl (2.028 Å). $[Ru(bpy)_2Cl_2]$ shows the same trend in Ru−N(bpy) distances (cf. 2.054 Å trans to N(bpy) and 2.014 Å trans to Cl).[67] The structure of a related trans-polypyridine complex, $[Ru(CH_3CN)(Cl)(o\text{-}bpy)_2]^+$ is known[68] and has Ru−N(bpy, trans to bpy) averaging 2.08(4) Å, albeit there is greater variation in equivalent distances and some evidence of strain. The Ru−N(NCCH$_3$) distance is shorter when trans to Cl (1.987 Å)[68] than trans to bpy (2.037 Å, this work). The Ru−Cl distance here (2.422 Å) is normal.[67,68]

Table 1. Crystal Data for $[Ru(CH_3CN)(Cl)(bpy)_2][CF_3SO_3]$

formula	$C_{23}H_{19}Cl_1F_3N_5O_3Ru_1S_1$
fw	639.01
space group, system	$P2_1/n$, monoclinic
a (Å)	9.2280(4)
b (Å)	18.4277(7)
c (Å)	15.1148(7)
β (deg)	91.010(2)
V (Å^3)	2569.9(2)
Z	4
temp (K)	100(2)
λ (Å)	0.71073
density, calcd (g cm^{-3})	1.652
μ (mm^{-1})	0.852
$R(F)$ (%)[a]	3.02
$Rw(F)$ (%)[a]	6.78

[a] $R(F) = \sum||F_o| - |F_c||/\sum|F_o|$; $Rw(F) = [\sum w(F_o^2 - F_c^2)^2/\sum w(F_o^2)^2]^{1/2}$ for $I > 2\sigma(I)$. $Rw(F) = [\sum w(F_o^2 - F_c^2)^2/\sum w(F_o^2)^2]^{1/2}$ for $I > 2\sigma(I)$.

Diffraction data for $[Ru(CH_3CN)(Cl)(bpy)_2][SO_3CF_3]$ were measured, and a summary of the crystallographic parameters is given in Table 1; further details can be found in the Supporting Information (S4) and at the Cambridge Crystallographic Data Centre.[39]

C. Instrumentation. Emission spectra in 77 K glasses were obtained as described in detail elsewhere[26,49] using a calibrated (Xe emission lines for wavelength and an Oriel model 63358 Quartz Tungsten Halogen QTH lamp for intensity) Princeton Instruments (Roper Scientific) OMA V InGaAs array detector (512 pixels) mounted on an Acton SP500 spectrometer with a 300 g/mm grating, blazed at 1000 nm. We have used first order dispersion in this instrument for complexes with emission maxima less than about 800 nm, and second order dispersion for complexes with higher energy emission maxima. There is some instrumental noise at ~1400 nm in the resulting second order emission spectra. We have also used a SPEX Tau2 Fluorimeter for general spectral characterizations of the higher energy emissions; unfortunately, the intensity response of this instrument did not prove to be sufficiently

(61) Dwyer, F. P.; Goodwin, H. A.; Gyarfas, E. C. *Aust. J. Chem.* **1963**, *16*, 544.
(62) Dixon, N. E.; Lawrence, A.; Lay, P. A.; Sargeson, A. M.; Taube, H. *Inorg. Synth.* **1986**, *24*, 243.
(63) Johnson, C. E.; Sullivan, B. P.; Salmon, J. D.; Adeymi, A. O.; Meyer, T. J. *Inorg. Chem.* **1978**, *17*, 2211.
(64) Sullivan, B. P.; Salmon, D. J.; Meyer, T. J. *Inorg. Chem.* **1978**, *17*, 3334.
(65) *APEX II, collection and processing programs*; Bruker AXS Inc.: Madison, WI, 2004.
(66) Sheldrick, G. *SHELX-97*; University of Göttingen: Göttingen, Germany, 1997.
(67) Eggleston, D. S.; Goldsby, K. A.; Hodgson, D. J.; Meyer, T. J. *Inorg. Chem.* **1985**, *24*, 4573.
(68) Masood, M. A.; Sullivan, B. P.; Hodgson, D. J. *J. Inorg. Chem.* **1994**, *33*, 4611.

Table 2. Spectral Components for Some $[Ru(L)_{6-2n}(bpy)_n]^{m+}$ Complexes[a]

ligands (m) [solvent]	$h\nu_{max(abs)}$, (ambient) cm^{-1}	$h\nu_{max(em)}$, (77 K) cm^{-1}	$h\nu_{max(f)}$, $\{\Delta\nu_{1/2}\}$[b]	$h\nu_{dmax(lf)}$, $[A_{max}]$ $\{\Delta\nu_{1/2}\}$[c]	$h\nu_{dmax(comb)}$, $[A_{max}]$ $\{\Delta\nu_{1/2}\}$[d]	$h\nu_{dmax(addOB3)}$, $[A_{max(added)}]$[e]	$h\nu_{dmax(OB3)}$, $[A_{max(initial)}]$[f]	$h\nu_{dmax(Ra)}$, $[A_{max}]$[g]	$h\nu_{dmax(Rb)}$, $[A_{max}]$[g]	(A_{lf}/A_{mf})[h]
$(bpy)_3$ (2)[alc][i]	22,200	17,128	17,224 {662}	430 [0.505] {666}	1870 [0.286] {822}	1436 [0.06]	1440 [0.506]	1070 [0.14]	2680 [0.11]	0.72
$(NH_3)_4$bpy (2) [bun][j]	19,000	12,341	12,493 {881}	490[0.49] {920}	1920[0.229] {1030}	1429[0.07]	1429[0.398]	1120 [0.03]	>2700 [0.03]	0.94
$(NH_3)_2(bpy)_2$ (2) [bun][j]	20,400	14,638	14,713 {745}	527 [0.45] {781}	1969 [0.203] {892}	1440 [−0.05]	1440 [0.502]	1100 [0.1]	>2500 [0.15]	0.87
$(en)(bpy)_2$(2)[bun][j]	20,200	15,110	15,213{638}	470[0.49]{601}	1910[0.228]{800}	1440[0.034]	1440[0.430]	1100 [0.16]	2500[0.05]	0.79
$([14]aneN_4)$bpy(2)[bun][k]	19,500	13,977	14,083{840}	460[0.46]{842}	1884[0.223]{980}	1424[0.065]	1424[0.420]	1125 [0.07]	2600 [0.042]	0.81
(trien)bpy(2) [bun][k]	19.500	12,981	13,050 {836}	475 [0.39] {949}	1902 [0.182] {976}	1430 [0.046]	1430 [0.42]	1220 [0.077]	2500 [0.06]	0.81
$([12]aneN_4)$bpy (2) [bun][k]	19,100	13,306	13,563{716}	345[0.915]{783}	1779[0.269]{902}	1434[−0.093]	1434[0.387]	1120 [0.18]	2400 [0.037]	2.7
$(py)_2(bpy)_2$ (2) [bun][i]	21,830	17,044	17,147 {641}	600 [0.40] {755}	2044[0.22]{846}	1444[0.055]	1444[0.500]	1110 [0.08]	2700 [0.09]	0.64
$(py)_4$bpy (2) [bun][k]	22,600	16,854	16,878 {780}	870 [0.31] {1079}	2308 [0.135] {964}	1438 [−0.152]	1438 [0.607]	1140 [0.03]	2000 [−0.06]	0.76
$(CH_3CN)_2(bpy)_2$ (2) [alc][i]	23,580	18,467	18,559v {678}	475 [0.46] {737}	1911 [0.338] {820}	1436 [0.15]	1436 [0.582]	1150 [0.11]	2460 [0.07]	0.56
$(CH_3CN)(Cl)$bpy (1) [alc][i]	21,300	15,689	15,813 {824}	545 [0.52] {790}	1979 [0.281] {988}	1434 [−0.02]	1434 [0.507]	∼1350 [0.2]	2500 [0.02]	0.82
$(CH_3CN)(Br)$bpy (1) [alc][i]	21,100	15,690	15,826 (881}	640[0.55]{782}	2072 [0.28] {1028}	1432 [−0.011]	1432 [0.506]	∼1300 [0.2]	2500 [0.0]	0.85
$(CH_3CN)(NCS)$bpy (1) [alc][i]	21,800	16,212	16,316 {1146}	680[0.41]{1031}	2101 [0.256]{1234}	1441[0.013]	1441[0.602]	∼2000 [∼0.04]		0.56
$(Cl)_2(bpy)_2(0)$ [alc][i]	19,080	14,283	14,468{833}	630[0.73]{834}	2068 [0.290] {968}	1432 [0]	1432 [0.399]	∼1090 [0.06]	>2600[0.1]	1.58
$(Br)_2(bpy)_2$ (0)[alc][i]	19,340	14,115	14,393 {971}	550 [0.690]{866}	1979[0.326] {1105}	1429 [0.077]	1429 [0.429]	none	2700 [0.07]	1.06
$(NO_2)_2(bpy)_2$ (0) [alc][i]	22,600	17,913	18,087 {1026}	940 [0.67] {971}	2383[0.446]{1160}	1443 [−0.17]	1443 [0.68]	1300[0.11]		0.82
$(CN)_2(bpy)_2$ (0) [alc][i]	21,600	16,837	16,971 {986}	950 [0.55] {1268}	2394 [0.255] {1120}	1444 [−0.03]	1444 [0.492]	1100−1300[0.007]		1.32
$(NCS)_2(bpy)_2$ (0) [alc][i]	20,120	14,665	14,847{1219}	880 [0.365] {1161}	2314 [0.17] {1344}	1434 [0.012]	1434 [0.445]	None	>2500 [>0.02]	0.83
$(C_2O_4)(bpy)_2$ (0) [alc][i]	19,290	14,117	14,196 {904}	730[0.395]{866}	2168 [0.191] {998}	1438 [0.051]	1438 [0.440]	1250[0.03]	2500−3000[<0.04]	0.75
$(C_3O_4H_2)(bpy)_2$ (0) [alc][i]	19,160	13,998	14,100{826}	660 [0.445] {781}	2102[0.18]{998}	1442 [-0.013]	1442 [0.422]	1139 [0.06]	>2600 [0.02]	0.85
$(CO_3)(bpy)_2$ (0) [alc][i]	18,480	13,947	14,034 {694}	560 [0.535] {666}	2004 [0.185] {842}	1444 [-0.007]	1444 [0.357]	1020 [0.08]	1780 [−0.02]	1.2

[a] All energies in units of cm^{-1}; all intensities relative to $I_{max(f)} = 1.000$. [b] Gaussian parameters for the fundamental component deconvoluted from the 77 K emission spectrum. [c] Gaussian parameters for a fitted *lf* component in the remainder spectrum. [d] Gaussian parameters for a *lf*/*mf* combination band: $h\nu_{max(comb)} = h\nu_{max(lf)} + h\nu_{max(1stOB3)}$ and $\Delta\nu_{1/2(comb)} = \Delta\nu_{1/2(lf)} + \Delta\nu_{1/2(1stOB3)}$ and "*1stOB3*" designates Gaussian parameters calculated for the envelope of 1st order vibronic components in the OB3 model. [e] Correction of $I_{\nu_m(OB3)}$ used to optimize the fit of $A_{\nu_m(rem)}$. [f] Calculated OB3 parameters. [g] Residual maxima: $A_{max(rem)} - A_{\nu_m}(lf1)$. [h] $A_{\rho f} = A_{max(\rho f)} \times \Delta\nu_{1/2(\rho f)}$. [i] This work; alc = 1:1 methanol:ethanol. [j] Spectra from ref 26; bun = butyronitrile. [k] Spectra from ref 27.

reliable for the band shape characterization of these complexes. Complexes were irradiated in their MLCT absorption bands using CW diode laser modules: 532 (50 mW) and 470 (5 mW) nm excitation was provided by MGL-S-B 50 mW modules (Changchun Industries Optoelectronics Tech Co. Ltd.) purchased from OnPoint Lasers, Inc.; 405 (50 mW) nm excitation was provided by a Power Technology, Inc. module; and 658 (65 mW) excitation was provided by a Newport LPM658−65E module. ASCII files were transferred to EXCEL and 10−30 spectra were averaged for each complex.

UV−visible spectra were recorded using a Shimadzu UV-2101PC spectrophotometer; ^{1}H and ^{13}C NMR spectra were obtained using a Varian 300 MHz instrument. The absorption spectra are presented in Supporting Information, Figure S5.[39]

Cyclic voltammograms (CV) were obtained in dry CH_3CN using a three-electrode system consisting of a Ag/AgCl reference electrode, a Pt wire counter electrode, and a Pt disk working electrode with a BAS model 100A electrochemical workstation for measurements. The solutions consisted of the complex dissolved in acetonitrile containing 0.1 mol/L tetrabutylammonium hexafluorophosphate as electrolyte. Ferrocene was dissolved in the sample solutions as an internal reference for the cyclic voltammograms. The electrochemical observations are summarized in Supporting Information, Table S6.[39]

D. Methods Used for the Analysis of the 77 K Emission Bandshapes. 1. General Information. The emission spectrum of a complex is interpreted as the sum of the intensities contributed by the radiative decay of an electronic excited state to each of the normal vibrational modes (k) of the ground state. These component intensities are functions of parameters characteristic of the differences in the molecular and electronic structures of the ground and excited states: (a) the vibrational quanta ($h\nu_k$) of the mode k; (b) the square of the displacements of the excited-state potential energy (PE) minimum in the normal coordinates of that mode (conveniently represented in terms of a vibrational reorganizational energy, λ_k); (c) symmetry constraints on the electronic or vibronic transitions (contained in an electronic matrix element H_{ij}). The localization of the electronic charge on different specific molecular functional groups in the ground and vibrationally equilibrated charge transfer excited states of a complex usually results in very low symmetry so that symmetry constraints can usually be ignored in interpreting the observed emission bandshapes, and these bandshapes can be reasonably straightforward probes of the excited-state molecular geometry.

When the ground and excited state differ in geometry only in the coordinates of the kth normal mode of the ground state and assuming Gaussian component bandshapes, the emission spectrum can be represented as[23,24,69,70]

$$(I_{\nu_m})_k = C\sum_j F_{j,k}[\mathrm{e}^{-\{4g_{j,k}^2 \ln 2/\Delta\nu_{1/2}^2\}}] \tag{4}$$

where

$$C = \frac{64\pi^4}{3h^3c^3 \ln 10}\frac{\nu_m\eta^3 H_{eg}^{\ 2}(\Delta\mu_{eg})^2}{(4\pi\lambda_s k_B T)^{1/2}} \tag{5}$$

$$F_{j,k} = \frac{S_k^{\ j}\mathrm{e}^{-S_k}}{j!} \qquad S_k = \frac{\lambda_k}{h\nu_k} \tag{6}$$

$$g_{j,k} = E_{eg}^{0'0} - \lambda_s - jh\upsilon_k - h\upsilon_m \tag{7}$$

In these equations, η is the index of refraction, ν_m is the frequency of the incident radiation, $(H_{eg}/h\nu_{eg})\Delta\mu_{eg}$ has been substituted for the transition dipole, M_{eg},[23,71,72] H_{eg} is the electronic matrix element, $\Delta\mu_{eg}$ is the difference between the excited-state and ground-state dipole moments, λ_s is the solvent reorganizational energy and other displacement modes with frequencies $\nu_s < 4k_BT$, and c is the speed of light. The component with $j = 0$ corresponds to the transition between the PE minima of the two states, $\{e,0'\}\rightarrow\{g,0\}$, with an intensity that can be represented as $I_{\nu_m(0'0)}$, where (note that $I_{max(0'0)}$ contains a factor of $\exp(-\sum_k S_k)$)[37−39]

$$I_{\nu_m(0'0)} \cong I_{max(0'0)}e^{\{-[E_{eg}^{0'0} - h\nu_m]^2/(\Delta\nu_{1/2}^2/4 \ln 2)\}} \tag{8}$$

This component makes the largest amplitude contribution to the emission spectra of most $[Ru(L)_4bpy]^{m+}$ complexes.[26,43,44] Distortions in a large number (>10) of different vibrational modes typically contribute to the emission bandshapes[36,40,41,73] and these contributions are not generally resolved in the 77 K emission spectra, so we have evolved systematic approaches for evaluating the contributions of different classes of distortion modes as suggested by eq 2 rather than the individual vibronic components.

2. Evaluation of the {e,0′} → {g,0} Contribution to the Emission Spectra. This contribution is not resolved in the 77 K emission spectra discussed here. Rather, we have determined a "fundamental emission component,"[26,37−39] $I_{\nu_m(f)}$, by means of a careful fitting of a Gaussian component to the high energy, dominant emission peak using Grams32 as discussed elsewhere,[26] and in the limit that $I_{\nu_m(0'0)}$ dominates the emission spectrum and/or there is very little overlap with vibronic components, $I_{\nu_m(f)} = I_{\nu_m(0'0)}$.[37] When there is a small amount of overlap with vibronic components, the fundamental component determined using Grams32 can be adjusted so that $I_{\nu_m(diff)}$ approaches zero smoothly for a better estimate of $I_{\nu_m(f)}$. The values of $h\nu_{max(f)}$ and $\Delta\nu_{1/2}$ determined for $I_{\nu_m(f)}$ have been used without change in the remaining analysis except as indicated.

3. Spectral Envelope of Vibronic Contributions: The Difference Spectrum. The difference spectrum in eq 1 is interpreted as the envelope of the convoluted vibronic components corresponding to the differences in the ground- and excited-state molecular geometries, and significant differences are usually found in some subset (i.e., the k distortion modes) of the normal vibrational modes. Thus, in principle the emission sideband and the difference spectrum consist of the sum of vibronic progressions in each of the k distortion modes (eq 3) plus the various combination bands that contain contributions from different modes. These vibronic components can be organized in various ways. We have previously represented the band shape in terms of the respective sums of first order, second order, third order, and so forth Gaussian component contributions ($I_{\nu_m(0'1)} + I_{\nu_m(0'2)} + I_{\nu_m(0'3)}$...; note that combination band as well as harmonic components are included in the higher order sums when there is no subscript denoting a distortion mode),[26,44] but this approach is not useful when the individual components are not resolved in the spectrum or available from rR studies. To approach the spectrum from the perspective represented in eq 2, we consider the intensity contribution of the kth distortion mode to be the sum over all components j of the corresponding vibronic progression; see eq 3. Thus, the emission intensity at a frequency

(69) Englman, R.; Jortner, J. *Mol. Phys.* **1970**, *18*, 145.
(70) Myers, A. B. *Acc. Chem. Res.* **1997**, *30*, 519.
(71) Yardley, J. T. *Introduction to Molecular Energy Transfer*; Academic: New York, 1980.
(72) Myers,A. B. In *Laser Techniques in Chemistry*; Myers, A. B., Rizzo, T. R., Eds.; John Wiley & Sons, Inc.: 1995; Vol. *XXIII*, p 325.
(73) Yersin, H.; Braun, D.; Hensler, G. ; Galhuber, E. In *Vibronic Processes in Inorganic Chemistry*; Flint, C. D., Ed.; Kluwer: Dordrecht, 1989; p 195.

ν_m is given by the sum of all of the progressions in the distortion modes plus the intensity contributions of combination bands (p,q; p,q,r; etc.)[26] so that the emission spectrum can be represented as

$$I_{\nu_m} \cong I_{\nu_m(0'0)} + \sum_k I_{\nu_{m(k)}} + \sum_{p,q} I_{\nu_{m(p,q)}} + \sum_{p,q,r} I_{\nu_{m(p,q,r)}} + \ldots \quad (9)$$

Rearranging eq 9 leads to

$$\left(I_{\nu_m} - I_{\nu_m(0'0)}\right) \cong \sum_k I_{\nu_{m(k)}} + \sum_{p,q} I_{\nu_{m(p,q)}} + \sum_{p,q,r} I_{\nu_{m(p,q,r)}} + \ldots \quad (10)$$

Equation 10 is then a theoretical basis for eq 2, with the vibronic components arranged by their order. The $I_{\nu_{m(f)}}$ component generated by our procedure is characterized by $h\nu_{max(f)}$ and $\Delta\nu_{1/2}$; we assume that $h\nu_{max(f)} \cong E_{ge}{}^{0'0}$ and that all vibronic components have the same $\Delta\nu_{1/2}$ bandwidth. Although the individual vibronic components are not resolved in the 77 K emission spectra, the envelopes of contributions in different spectral regions are often evident in the difference spectra (see Figure 2),[27,48] or in the differences in emission bandshapes for the isotopomers of some complexes.[26,28,47,49] The terms of eq 10 can be regrouped to emphasize the emission sideband contributions that arise predominately from distortions in different functional groups of the molecule (as in eq 2)

$$I_{\nu_{m(sideband)}} \cong \sum_g \left(I_{\nu_m(0'1)} + I_{\nu_m(0'2)} + I_{\nu_m(0'3)} + \ldots\right)_g + \sum_{p,q(\nu_p \neq \nu_q)} I_{\nu_{m(p,q)}} + \ldots \quad (11)$$

The first summation in eq 11 is over all distortion modes of functional groups within the molecule (e.g., vibrational modes that are largely those of the bpy ligand, the metal−ligand skeletal modes, the intraligand modes of spectator ligands, etc.), and the last term takes account of the second order intergroup combination band contributions. We have found that the spectral combination band intergroup contributions are very important in determining the emission bandshapes.[26] Equation 11 is a useful approximation only when the atomic motions within different functional groups are not strongly coupled in the normal vibrational modes of the complex. Thus, this approximation will be most useful when the vibrational frequencies characteristic of different functional group differ greatly, when the functional groups are not intimately linked within the complex, or when the vibrational mixing is symmetry forbidden.

4. Evaluation of the Vibronic Contributions Arising from Distortions in Predominately bpy-Localized Vibrational Modes: The OB3 Model. The rR parameters reported (see Supporting Information, Table S1)[39] for the structurally similar complexes $[Ru(bpy)_3]^{2+}$[40] and $[Os(bpy)_3]^{2+}$[36] suggest that the distortions in the predominately bpy-localized vibrational modes are very similar and that the distortions in the metal−ligand-localized vibrational modes are very different as is shown in Figure 3. Of course, there are some relatively small differences (see Supporting Information, Figure S7)[39] in the *mf* rR parameters for these complexes and these could arise from any combination of the following: (a) differences in vibronic attenuation due to MLCT/ground-state or MLCT/other-excited-state configurational mixing; (b) differences in the amplitudes of intergroup combination bands; and/or (c) variations in the molecular vibrational mode frequencies and distortion amplitudes that arise from the coupling of the metal−ligand and bpy-centered vibrational motions. However, substantial distortions in metal−ligand vibrational modes are a characteristic of $[Ru(bpy)_3]^{2+}$ but not of $[Os(bpy)_3]^{2+}$, and this comparison strongly supports the group frequency approach to vibronic analysis represented by eq 2. Furthermore, the very dramatic difference in the distortion amplitudes of these complexes in the *lf* regime suggests that the $[Os(bpy)_3]^{2+}$ rR parameters can be used as a good approximation to the bandshapes expected for distortions in largely bpy-localized vibrational modes in the limit that there is no configurational mixing between the ^{3}MLCT excited state and other electronic excited states of a $[(L)_4M(bpy)]^{m+}$ complex (OB3 model; details summarized in Supporting Information, S8).[39] Thus, we have employed the $[Os(bpy)_3]^{2+}$[36] rR parameters throughout this paper to model the contributions expected to arise from distortions in largely bpy-localized vibrational modes. However, configurational mixing between the MLCT excited state and the ground state can decrease the difference between the nuclear coordinates of the PE minima of these states, and this results in decreases in the amplitudes of the corresponding vibronic contributions to the spectra.[26,74,75] For a two state system involving a single donor and a single acceptor (and for $\alpha_{ij}^2 < 0.1$), this attenuation of the intensity in the vibronic sidebands can be expressed in terms of the reorganizational energy contributions to the displacement modes,[26–28,43,44,74–78]

$$\lambda_r \cong \lambda_r^o\left(1 - 2\alpha_{ge}^2 - 2\alpha_{eg}^2\right) \quad (12)$$

where the $\alpha_{ij} = H_{ij}/E_{ij}$ are normalized coefficients for mixing the respective diabatic wave functions evaluated at the coordinates of the ground state (*ge*) and excited state (*eg*) PE minima. Because values of H_{ij} for Ru(II) donors and pyridyl or polypyridyl acceptors are in the range of 6000−11 000 cm^{-1} and MLCT excited-state energies are generally less than 25 000 cm^{-1},[75,79,80] significant vibronic attenuation must be considered. Equation 12 is the basis for empirical correlations of the observed variations in vibronic amplitudes with excited-state energies,[26–28,43,44,50] and in the OB3 modeling we have based the attenuation factors on the difference in rR parameters reported for bpy vibrational modes of the $[Ru(bpy)_3]^{2+}$[40] and $[Ru(NH_3)_4bpy]^{2+}$[41] complexes. Thus, a correction factor f is constructed for each complex with,[26,43,44,50]

$$f = \frac{\left(1 - \dfrac{0.227 \times 10^9}{h\nu_{max(abs)}^2}\right)_{complex}}{\left(1 - \dfrac{0.227 \times 10^9}{h\nu_{max(abs)}^2}\right)_{[Ru(bpy)_3]2+}} \quad (13)$$

We then construct an envelope of the sum of first and second order vibronic intensity contributions based on Gaussian functions with the bandwidth of the fundamental component deconvoluted from the observed emission spectrum, and with Huang−Rhys parameters $S_k = f\,S_k'$.

(74) Endicott, J. F.; Uddin, M. J.; Schlegel, H. B. *Res. Chem. Intermed.* **2002**, *28*, 761.
(75) Seneviratne, D. S.; Uddin, M. J.; Swayambunathan, V.; Schlegel, H. B.; Endicott, J. F. *Inorg. Chem.* **2002**, *41*, 1502.
(76) Matyushov, D. V.; Voth, G. A. *J. Phys. Chem. A* **2000**, *104*, 6470.
(77) Matyushov, D. V.; Newton, M. D. *J. Phys. Chem. A* **2001**, *105*, 8516.
(78) Endicott, J. F.; Schegel, H. B.; Uddin, M. J.; Seneviratne, D. *Coord. Chem. Rev.* **2002**, *229*, 95.
(79) Coe, B. J.; Harris, J. A.; Brunschwig, B. S.; Asselberghs, I.; Clays, K.; Garin, J.; Orduna, J. *J. Am. Chem. Soc.* **2005**, *127*, 13399.
(80) Shin, Y. K.; Brunschwig, B. S.; Creutz, C.; Sutin, N. *J. Phys. Chem.* **1996**, *100*, 8157.

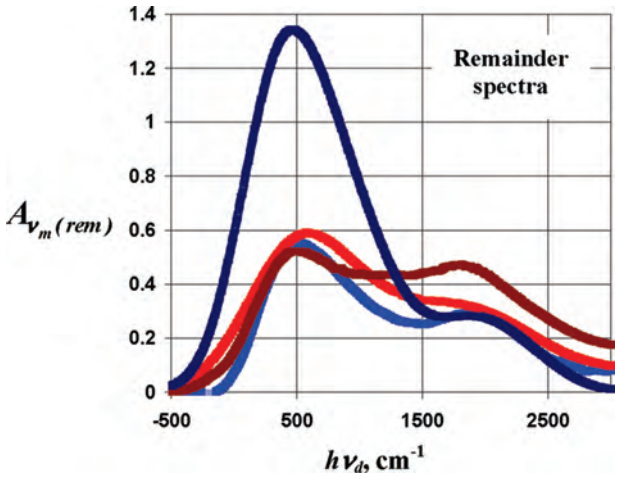

Figure 5. Comparisons of the "remainder" vibronic contributions to 77 K emission bandshapes, $A_{\nu_m(rem)} = A_{\nu_m(diff)} - (A_{\nu_m(0'1)} + A_{\nu_m(0'2)} + A_{\nu_m(0'3)} + ...)_{OB3}$, for $[Ru(bpy)_3]^{2+}$ (red), $[Ru(NH_3)_4bpy]^{2+}$ (blue), $[Ru(CH_3CN)_2(bpy)_2]^{2+}$ (dark red), and $[Ru([12]aneN_4))bpy]^{2+}$ (dark blue); see also Figures 1 and 2.

It is important to observe that the variable parameters used in the OB3 model are those of $I_{\nu_m(f)}$ ($\Delta\nu_{1/2}$, $h\nu_{max(f)}$, and $I_{max(f)}$) and f (obtained from an independent empirical correlation) which estimates the attenuation of these sideband amplitudes as a result of configurational mixing with the ground state.

5. Evaluation of the Vibronic Contributions Arising from Distortions in Predominately Metal−Ligand Vibrational Modes. The removal of the contributions of the bpy distortion modes from the normalized difference spectrum results in a normalized "remainder" spectrum, $A_{\nu_m(rem)} \cong A_{\nu_m(diff)} - (A_{\nu_m(0'1)} + A_{\nu_m(0'2)})_{OB3}$, which emphasizes the vibronic contributions that result from those excited-state distortions that are largely localized in other functional groups of the molecule,[37]

$$A_{\nu_m(rem)} \cong \frac{1}{I_{max(f)}}\left[\sum_{other}\left(I_{\nu_m(0'1)} + I_{\nu_m(0'2)} + I_{\nu_m(0'3)} + ...\right)_{other} + \sum_{\substack{all\ inter\text{-}gp.\ comb's \\ i,j(\nu_i \neq \nu_j)}}\left(I_{\nu_{(i+j)}} + I_{\nu_{(2i+j)}} + ...\right) + ...\right] \quad (14)$$

Figure 5 shows the remainder spectra that are generated from the emission spectra in Figure 1 using the OB3 model to estimate $I_{\nu_m(bpy)}$. Many of the remainder spectra of the complexes considered here have their dominant vibronic contributions in the 300−600 cm^{-1} region that is characteristic of metal−ligand vibrational modes. We have used an empirical fitting approach to evaluate variations in the *lf* contributions to Ru-bpy emission spectra in this report, but there are some important points that must be considered before we develop those details: (a) The sideband amplitudes must decrease with decreasing MLCT excited-state energy more or less as described by eq 12,[26–28,43,44,50,51] and this accounts for some of the band shape variation shown in Figures 1 and 2 (the emission band shape of $[Ru([12]aneN_4)bpy]^{2+}$ is an obvious exception). (b) Modeling with rR parameters indicates that higher order vibronic contributions, including combination bands, make very important contributions to the emission bandshapes.

It is to be noted that the amplitudes of the normalized vibronic envelopes in Figures 2 and 5 are larger ($A_{max(g)} > 0.4$) than allowed for a single vibronic component by eq 6 and $I_{\nu_m(f)}$.[37] The large vibronic amplitudes of these complexes arise from the overlapping contributions of many individual components whose energy differences are small compared to $\Delta\nu_{1/2}$ as is illustrated by Figure 3 and has been discussed previously.[26] Thus, one must be cautious in interpreting the parameters obtained from empirical "equivalent mode" fittings. With these points in mind, we use the fittings described below to examine variations in excited-state distortions in related series of complexes.

Provided that the fundamental component is properly evaluated, the spectral representations based on eq 10 should lead to envelopes that can be interpreted in terms of eq 11. The large amplitudes of the vibronic envelopes in any particular spectral region are the result of the overlap of many components whose difference in energy is smaller than $\Delta\nu_{1/2}$.[26] For a single distortion mode model eq 11 reduces to

$$I_{\nu_m(sideband)} \cong C\sum_j \frac{S^j e^{-S}}{j!}[e^{-\{4g_j^2 \ln 2/\Delta\nu_{1/2}^2\}}] \quad (15)$$

Because the normalized (eq 1) vibronic envelopes (Figures 2 and 5) have large amplitudes, they tend to require that $j = 1$ for the largest amplitude component of any progression in an "equivalent" mode (see above and Supporting Information, S8 and S9).[37,39] Furthermore, the importance of higher order vibronic contributions that has been demonstrated in the rR modeling of the $[Ru(bpy)_3]^{2+}$ and $[Ru(NH_3)_4bpy]^{2+}$ emission spectra[26] suggests that any reduced or "equivalent" mode model must retain some features of vibronic progressions. We have based our empirical approach on a more detailed rR modeling of the emission spectral features of these complexes.

6. Procedure for Comparing Low Frequency Vibronic Contributions to the Emission Spectra of Ru-bpy Chromophores (*lf*1 Model). Overall, the procedure that we employ here amounts to evaluating the difference spectrum in terms of the contributions from two classes of distortion modes: (a) the distortions associated with a "pure" Ru-bpy MLCT excited state evaluated by means of the rR-based OB3 model; and (b) a best fit modeling of *lf* vibronic contributions by means of an approach based on a comparison of the $[Ru(NH_3)_4bpy]^{2+}$ remainder spectrum to the reported rR parameters[41] (*lf*1 model). Briefly summarized, our *lf*1 approach is as follows: (a) Construct a remainder spectrum of vibronic components, $A_{\nu_m(rem)} = A_{\nu_m(diff)} - A_{\nu_m(OB3)}$. (b) Deconvolute $A_{\nu_m(rem)}$ into 3−4 Gaussian contributions using Grams32, optimizing the fit of a Gaussian component to the largest amplitude, lowest frequency feature of the envelope, $G_{m(lf)}$ (maximum amplitude $A_{max(lf)}$ at $h\nu_{max(lf)}$ and with a bandwidth of $\Delta\nu_{1/2(lf)}$). (c) Construct a "progression", $A_{\nu_m(lf1)}$, in $G_{m(lf)}$ and its combinations with bpy modes (B) obtained from the OB3 model parameters,

$$A_{\nu_m(lf1)} = G_{\nu_m(lf)} + G_{\nu_m(lf2)} + G_{\nu_m(lf3)} + G_{\nu_m(lf*B)} + G_{\nu_m(lf2*B)} + G_{\nu_m(lf*B2)} + \partial A_{\nu_m(OB3)} \quad (16)$$

The Gaussian functions in eq 16 are constructed for a best fit of the remainder spectrum by adjusting $h\nu_{max(lf)}$, $\Delta\nu_{1/2(lf)}$ and $A_{max(lf)}$ of the $G_{m(lf)}$ component; the higher order terms so generated approximate a vibronic "progression" in the *lf*mode. The higher terms (Gaussian parameters) in the *lf* "progression" are based on a best fit to the envelope of *lf* rR-based components for $[Ru(NH_3)_4bpy]^{2+}$: $G_{m(lf2)}$ ($2h\nu_{max(lf)}$, $\Delta\nu_{1/2(lf)}$, and $1.3[A_{max(lf)}]^2/2$) and $G_{m(lf3)}$ ($3h\nu_{max(lf)}$, $\Delta\nu_{1/2(lf)}$, and $1.3[A_{max(lf)}]^3/6$) and not consistent with eqs 4–7.[37] The intergroup combination band contributions (designated by * in the subscript) are based on a Gaussian fit, $G_{m(B)}$ (with $h\nu_{max(B)}$, $\Delta\nu_{1/}$

$_{2(B)}$, and $I_{max(B)}$) to the envelope of first order $[Os(bpy)_3]^{2+}$ rR-based vibronic contributions to the OB3 model for the complex. Thus, for: $G_{m(lf*B)}$, $h\nu_{max(lf*B)} = (h\nu_{max(lf)} + h\nu_{max(B)})$, $\Delta\nu_{1/2(lf*B)} = \Delta\nu_{1/2(B)}$ and $A_{max(lf*B)} = (A_{max(lf)} \times A_{max(B)})$; $G_{m(lf2*B)}$, $h\nu_{max(lf2*B)} = (2h\nu_{max(lf)} + h\nu_{max(B)})$, $\Delta\nu_{1/2(lf*B)} = \Delta\nu_{1/2(B)}$ and $A_{max(lf*B)} = ([A_{max(lf)}]^2 \times A_{max(B)})/3$; *and* $G_{m(lf*B2)}$, $h\nu_{max(lf*B)} = (h\nu_{max(lf)} + 2h\nu_{max(B)})$, $\Delta\nu_{1/2(lf*B)} = \Delta\nu_{1/2(B)}$ and $A_{max(lf*B)} = (A_{max(lf)} \times [A_{max(B)}]^2)/3$. Finally we introduce a correction, $\partial A_{\nu_m(OB3)}$, for possible errors in the estimate of $A_{\nu_m(OB3)}$; this term is expected to be small (i.e., small values of $\partial A_{\nu_m(OB3)}$ indicate a good fit). The Gaussian parameters of $G_{m(lf)}$ ($h\nu_{max(lf)}$, $\Delta\nu_{1/2(lf)}$, $A_{max(lf)}$) and $\partial A_{\nu_m(OB3)}$ are adjusted to minimize the residuals. A relative residual, $[(A_{\nu_m(rem)} - A_{\nu_m(lf1)})/A_{\nu_m(em)}]$, is used as one measure of fit quality in Supporting Information, Table S11,[39] since the limiting uncertainty in component resolution is determined by uncertainties in the original spectral measurement.

To assess the uncertainties in this approach to interpreting band shape variations, we have (a) constructed hypothetical spectra for various bandwidths using the reported[41] $[Ru(NH_3)_4bpy]^{2+}$ rR parameters; (b) fitted these spectra using the procedures outlined above; and (c) compared the component contributions and spectra constructed from the rR parameters to those inferred from our fitting procedure. The results of this modeling are summarized in Supporting Information, S10[39] and indicate that the uncertainties in the determination of parameters for the envelope of *lf* vibronic contributions are 3−4%, and within this range of uncertainties we found no significant bandwidth dependence.

The patterns of deviations found here for the rR-modeled $[Ru(NH_3)_4bpy]^{2+}$ spectra provide a basis for the systematic comparison of the *low frequency* vibronic contributions to the spectra of the $[Ru(Am)_{6-2n}(bpy)_n]^{2+}$ series of complexes, since one would not expect dramatic differences among their distortion coordinates. When large deviations do occur, as for the $[Ru([12]aneN_4)bpy]^{2+}$ complex, then comparison to the $[Ru(Am)_{6-2n}(bpy)_n]^{2+}$ series of complexes may provide insight into the origin of those deviations. In general our approach depends on a reliable estimate of the fundamental component, and the rR modeling indicates that for $[Ru(NH_3)_4bpy]^{2+}$ this is generally possible if $\Delta\nu_{1/2} < \sim 1000$ cm^{-1} but not if $\Delta\nu_{1/2} > \sim 1000$ cm^{-1}. Furthermore, when the excited state is greatly distorted or when there are large amplitude vibronic contributions from distortions in vibrational modes for which $h\nu_k < \sim{}^1/_2\Delta\nu_{1/2}$, then our procedures will not result in good estimates of $I_{\nu_m(f)}$.

Results Section

In this study we have determined spectra for 11 $[Ru(L)_4bpy]^{m+}$ complexes in addition to the 10 spectra that were selected from our previous studies[26,27] to have a wide range "spectator" of ligands $(L)_4$. The absorption and emission maxima of these complexes span energy ranges of 4600 cm^{-1} and 6000 cm^{-1}, respectively, and their 77 K emission spectra exhibit a very wide range of bandshapes, but the bandshapes within each class of spectator ligands are generally very similar. Thus, there is more than a 3-fold range in the amplitudes of the sideband contributions relative to that of the highest energy emission feature of the 77 K emission spectra, from about 15% larger to 65% smaller than for the $[Ru(NO_2)_2(bpy)_2]$ and $[Ru([12]aneN_4)bpy]^{2+}$ complexes, respectively (e.g., see Figure 1), and the maximum sideband amplitudes occur for $h\nu_{max(diff)} \approx 450-1440$ cm^{-1} lower energy than $h\nu_{max(f)}$ for $[Ru([12]aneN_4)bpy]^{2+}$ and $[Ru(bpy)_3]^{2+}$, respectively. The 77 K emission sidebands (or difference spectra) of all of the $[Ru(Am)_{6-2n}(bpy)]^{2+}$ complexes examined here exhibit significant vibronic contributions in the $h\nu_{max(diff)} \approx 500$ cm^{-1} region that is typical of Ru-ligand vibrational modes as well as in the $h\nu_{max(diff)} \approx 1450$ cm^{-1} region that is expected for vibrational modes of the bpy ligand.

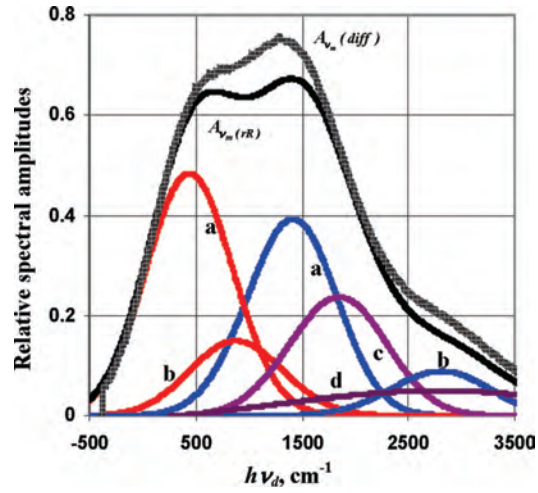

Figure 6. Comparison of the observed 77 K difference spectrum (thick black curve) for $[Ru(NH_3)_4bpy]^{2+}$ in butyronitrile to the sum of vibronic envelopes calculated from reported rR components (black curve). The vibronic envelopes calculated from rR parameters for the 1st and 2nd order contributions of the *lf* (red; $h\nu_{lf} < 1000$ cm^{-1}) and *mf* (blue; $h\nu_{mf} > 1000$ cm^{-1}) vibrational modes are indicated separately. The vibronic components, *k*, assume that $\Delta\nu_{1/2} = 891$ cm^{-1} and (**a**) $\sum_j S_j e^{-S_j} e^{-(\nu_{vib}-\nu_j)^2/w^2}$; (**b**) $\sum_j (S_j^2/2) e^{-S_j} e^{-(\nu_{vib}-2\nu_j)^2/w^2}$; (**c**) $\sum_{lf}\sum_{mf} (S_{lf}S_{mf}/2) e^{-(S_{lf}+S_{mf})/2} e^{-(\nu_{vib}-\nu_{lf}-\nu_{mf})^2/w^2}$ (violet); (**d**) approximate sum of 3rd order components (purple).

A. Fit of rR Parameters to the Difference and the Separation of the Contributions of *lf* and *mf* Vibrational Modes. 1. $[Ru(NH_3)_4bpy]^{2+}$. Figure 6 demonstrates that the envelope of rR-based vibronic contributions,

$$A_{\nu_m(rR)} = \sum_k S_k e^{-S_k} e^{-(\nu_k-\nu_{vib})^2/w^2} + \sum_j \sum_k \frac{S_j S_k}{2} e^{-(S_j+S_k)/2} e^{-(\nu_{vib}-\nu_j-\nu_k)^2/w^2} + \ldots = A^{(1)} + A^{(2)} + \ldots \quad (17)$$

fits the experimental difference spectrum very well (see also Supporting Information, S12). The sums of the *lf* ($h\nu_k < 1000$ cm^{-1}) and *mf* ($h\nu_k < 1000$ cm^{-1}) vibronic contributions have been carried out to 2nd order (eq 17), as indicated by labels on the envelopes in Figure 6, and 3rd order contributions have been estimated using an rR-based[26] polynomial (Supporting Information, S13).[39] The overall fit of $A_{\nu_m(rR)}$ to $A_{\nu_m(diff)}$ is very good. The calculated envelope, $A_{\nu_m(rR)}$, is systematically smaller than the experimental $A_{\nu_m(diff)}$ amplitudes in the regions of $h\nu_d \cong 500-1500$ cm^{-1} and ≥ 2500 cm^{-1}, and these discrepancies are <20% of the emission amplitude (Supporting Information, S11 and S12).[39] Random discrepancies of ≤10% between the observed difference spectrum and that calculated from rR parameters would not be surprising. On the other hand, the most likely sources of systematic differences are either (a) small systematic errors in our estimates of $I_{\nu_m(f)}$; and/or (b) that the vibronic parameters appropriate for absorption

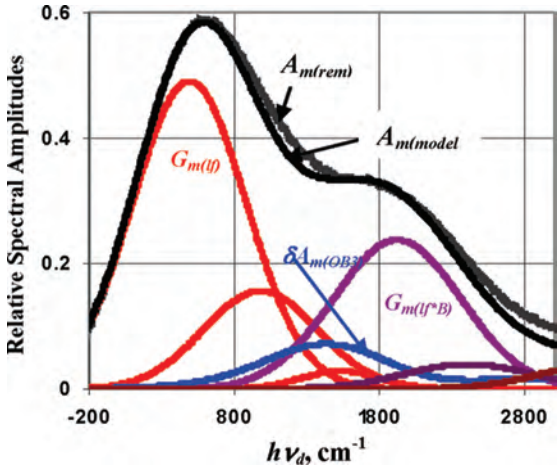

Figure 7. Comparison of the *lf*1 model to the remainder spectrum of $[Ru(NH_3)_4bpy]^{2+}$. The experimental remainder spectrum is the thick black line, and the sum of the components for the *lf*1 model is the solid black line. The progressions in the "equivalent" *lf* vibrational mode are in red; the *lf*/*mf* combination bands are violet and dark red; the $\partial A_{\nu_m(OB3)}$ term is in blue.

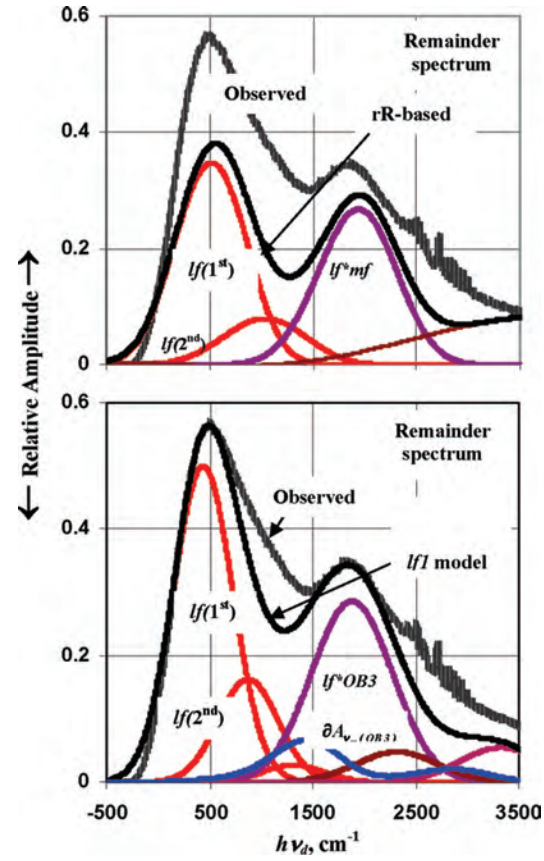

Figure 8. Comparison of the observed and calculated 77 K remainder spectra of $[Ru(bpy)_3]^{2+}$. Top panel: observed (thick gray lines) and rR-modeled. Bottom panel: observed (thick gray lines) and (*lf*1 + OB3) modeled. The 3rd order components are presented but not labeled (the dark red curve in the top panel is based on a polynomial fitting of 3rd order rR terms). The thick black lines are the overall calculated vibronic contributions. Components are color coded as in Figures 6 and 7.

and emission are different possibly because the rR parameters are for the Franck−Condon ^{1}MLCT excited state while the emission spectra are for the vibrationally equilibrated ^{3}MLCT excited state. Some of the higher frequency discrepancies can be attributed to the approximations of the 3rd order (and neglect of higher order) contributions (see Supporting Information, S13).

The *lf*1 model has been optimized to fit the $[Ru(NH_3)_4bpy]^{2+}$ remainder spectrum in Figure 7, and this is the basis for much of the following discussion. The $\partial A_{\nu_m(OB3)}$ correction of about 10% compares well with the 8% smaller amplitude of the envelope of *mf* contributions calculated from the rR parameters of $[Os(bpy)_3]^{2+}$ than those calculated for $[Ru(bpy)_3]^{2+}$ (see Figures 3 and Supporting Information, S12).[39]

2. $[Ru(bpy)_3]^{2+}$. We have previously found that emission spectral fits of the reported rR parameters[40,41] are much better for $[Ru(NH_3)_4bpy]^{2+}$ than for $[Ru(bpy)_3]^{2+}$.[26] This contrast is more evident in the more detailed fits considered here as is illustrated in Figure 8. Among the possible origins of the poorer quality fits of the $[Ru(bpy)_3]^{2+}$ than the $[Ru(NH_3)_4bpy]^{2+}$ emission spectrum are the following: (a) possible errors that arise from the use of Savin's rule to evaluate the atomic displacements from the rR spectra;[41] (b) a difference in the symmetry constraints for the vibronic contributions to rR and emission; and (c) a difference in the extent of LF/MLCT configurational mixing for the Franck−Condon and emitting excited states. The use of Savin's rule to evaluate the displacements based on the rR spectrum of $[Ru(NH_3)_4bpy]^{2+}$ apparently overestimates the amplitudes of the contributions of *lf* vibrational modes,[41] and this suggests that correcting for this effect would result in a significantly worse fit of the corresponding rR parameters to the emission spectrum of $[Ru(bpy)_3]^{2+}$. In this case the $\partial A_{\nu_m(OB3)}$ correction of about 10% is in good agreement with the difference in amplitudes of *mf* rR envelopes for $[Os(bpy)_3]^{2+}$ and $[Ru(bpy)_3]^{2+}$ in Figure 3. This suggests that the reported[40] rR parameters seriously underestimate the *lf* vibronic (but not *mf*) contributions to the $[Ru(bpy)_3]^{2+}$ emission spectrum. While the (*lf*1 + OB3) fitting substantially underestimates the vibronic amplitudes in the $\nu_d = 1000-1400$ cm^{-1} region (see Supporting Information, Figure S11),[39] this is at least qualitatively consistent with the smaller values of the $[Os(bpy)_3]^{2+}$ than $[Ru(bpy)_3]^{2+}$ S_k parameters reported for this spectral region.[36,40]

The idealized symmetry considerations summarized in Supporting Information, Table S13[39] do suggest that complications are possible in the analysis of the $[Ru(bpy)_3]^{2+}$ spectra. Thus, the Franck−Condon principle dictates that light absorption generates an excited state (the Franck−Condon excited state) which has the ground-state nuclear coordinates and D_3 symmetry (see Figure 9). While the lowest energy MLCT excited state may have A_2 (in C_2) symmetry and an $\{a_1(d\pi),a_2(LUMO)\}$ electronic configuration, the lowest energy allowed electronic transitions must generate Franck−Condon MLCT excited states with either E or A_1 symmetry (in D_3) and either $\{a_1(d\pi),e(LUMO)\}$, $\{e(d\pi),a_2(LUMO)\}$ or $\{e(d\pi),e(LUMO)\}$ electronic configurations. However, only the A_1 component with the $\{e(d\pi),e(LUMO)\}$ configuration can be configurationally mixed with the ground state, and this is likely to be the most intense component in the observed absorption spectrum and probed by rR. Similarly, the lowest energy LF excited state probably has E symmetry in the D_3 point group and should not mix significantly with

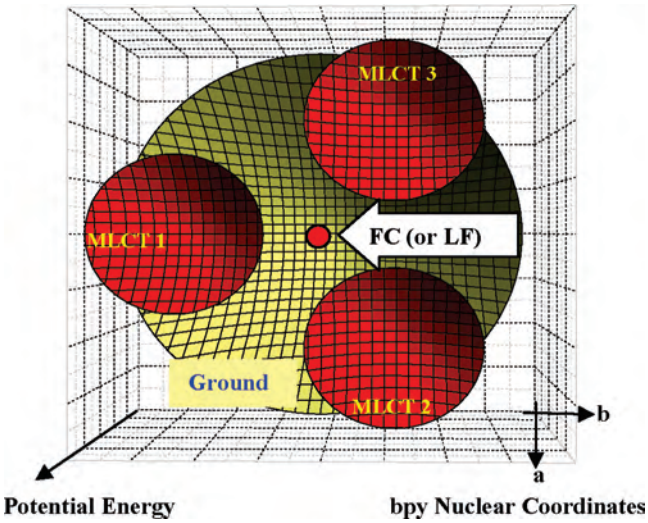

Figure 9. Qualitative illustration of the relationships between the diabatic ground electronic state, the three equivalent diabatic MLCT excited states, the Franck−Condon excited state (FC; nuclear coordinates of the ground-state PE minimum) or a higher energy ligand field state (LF; PE minimum at **a** = **b** = 0) of a $[M(bpy)_3]^{m+}$ complex. The view in this figure is along the PE axis. Two general nuclear coordinates (**a** and **b**) representing bpy distortions have been used for simplicity in this illustration although at least three would be required for the diabatic limit and a much larger number are implicated by rR[36,40,41] and high resolution 2 K emission studies.[73]

the A_1 (MLCT) Franck−Condon excited state (see Supporting Information, Table S13). These symmetry constraints may be partly relaxed by spin orbit coupling in the Franck−Condon excited state, and they are largely relaxed in a ^{3}MLCT excited state with the electron localized on a single bpy ligand (C_2 symmetry) so that much more ^{3}LF/^{3}MLCT configurational mixing is expected, consistent with the contrasts between the rR and emission spectral observations.

In addition to the above considerations, the LF and MLCT excited-state energy differences in the triplet manifolds that are probed by emission can be significantly different from those in the singlet manifolds that are probed by absorption or rR spectroscopy because the singlet−triplet energy difference for a given electronic configuration depends on the electron exchange energy, and the exchange energies of the ^{3}LF and ^{3}MLCT excited states are expected to be different; furthermore the exchange energies of $[Ru(NH_3)_4bpy]^{2+}$ tend to be significantly larger than those of $[Ru(bpy)_3]^{2+}$[81] so that the relative LF and MLCT energies within these manifolds may be different for the two complexes.

3. Some General Observations. The detailed fits of rR parameters to the $[Ru(NH_3)_4bpy]^{2+}$ emission band shape are very good. While the *lf*1 model is optimized to fit the bandshapes of this complex, there is still a significant deviation ($A_{max(res)} = 0.11$) near to $h\nu_d = 1200$ cm^{-1}, and a deviation from the *lf*1 fit in this region is observed in many of the complexes that we have examined. The rR parameters indicate that the vibronic contributions at $\nu_d \approx 1230$ cm^{-1} are about 0.1 larger (for $\Delta\nu_{1/2}$ 620 cm^{-1}) for $[Ru(bpy)_3]^{2+}$ than for $[Os(bpy)_3]^{2+}$ in this region (see Supporting Information, Figure S6),[39] and this arises from smaller Huang−Rhys parameters of the Os ($S_k = 0.062$ and 0.073 at 1174 and 1323 cm^{-1}, respectively)[36] than the Ru ($S_k = 0.115$ and 0.0.157 at 1176 and 1320 cm^{-1}, respectively)[40] complex. Thus, the OB3 model would tend to under represent the intensities in this region. The reason for this contrast in rR parameters is not clear, but some of these vibrations may correspond to molecular vibrational modes that couple local bpy and metal−ligand skeletal modes (or their overtones; the *lf*1 model assumes that the functional group vibrations are only weakly coupled). The amplitudes observed for the 1000−1300 cm^{-1} range features depend strongly on the bandwidth since the *lf* component found in the *lf*1 fits will overlap with them when $\Delta\nu_{1/2}$ is large and/or $h\nu_{max(lf)} > \sim$ 600 cm^{-1}, thereby reducing their apparent contribution to the band shape. The $\delta I_{m(OB3)}$ correction will also partly compensate for such contributions. In evaluating the quality of the *lf*1 fits we have considered the extent to which the inferred value of $h\nu_{max(lf)}$ differs from the expectation for a typical metal−ligand vibration (~450 cm^{-1}), the percentage of the OB3 correction required, and the deviation of the fit from the observed spectrum; see Supporting Information, Table S11.[39] In evaluating the deviations from the fit it is important to note that the OB3 model (which includes the approximate corrections for attenuation based on eq 12) is an idealized approximation to the vibronic contributions of bpy modes and deviations of ±10% are not unreasonable; note especially that we do not optimize the amplitudes of the $[Os(bpy)_3]^{2+}$ rR components to fit the spectral envelope based on $[Ru(bpy)_3]^{2+}$ rR parameters (see Figure 3).

B. Modeled Bandshapes of Other $[Ru(Am)_{6-2n}(bpy)_n]^{2+}$ Complexes. The spectral fittings for these complexes are summarized in Table 1 and presented in Figures 7, 8, and 10. In all cases, the fitted values of $h\nu_{max(lf)}$ are reasonable for the vibronic envelope of metal−ligand skeletal contributions; the bandwidths of the fitted *lf* Gaussian components are usually comparable to those of the fundamental, and the emission bandshapes are very similar. The major deviations found for these complexes are in the intermediate and *mf* regimes: (1) for $[Ru(NH_3)_2(bpy)_2]^{2+}$, a residual of 0.08 at about 1200 cm^{-1} and about a 1% OB3 correction; (2) for $[Ru(en)(bpy)_2]^{2+}$, a large residual of 0.16 at about 1100 cm^{-1} and about a 10% OB3 correction; (3) for $[Ru([14]aneN_4)bpy]^{2+}$, a residual of 0.07 at about 1150 cm^{-1} and a 11% OB3 correction; (4) for $[Ru(trien)bpy]^{2+}$, a residual of 0.08 at about 1250 cm^{-1}, an 11% OB3 correction; and the bandwidth of the $A_{\nu_m(lf)}$ is somewhat larger than that of $I_{\nu_m(f)}$. The small variations in these bandshapes probably result mostly from the variations in excited-state energies, vibronic component attenuation (eq 12), and component bandwidths. Overall, the *lf*1 modeling provides good fits up to $h\nu_d$ about 2300 cm^{-1}. In all cases the residual contribution in the 1100−1300 cm^{-1} range is usually the largest deviation between the fits and the difference spectra for $h\nu_d < 2000$ cm^{-1}; the mean sum of this contribution plus $\delta A_{m(OB3)}$ is 0.13 ± 0.06 (~20 ± 9% of the sideband intensity at ~1200 cm^{-1}) for this series. Note that the *lf*1 model does take account of at least some of the 3rd order

(81) Lever, A. B. P.; Gorelsky, S. I. *Coord. Chem. Rev.* **2000**, *208*, 153.

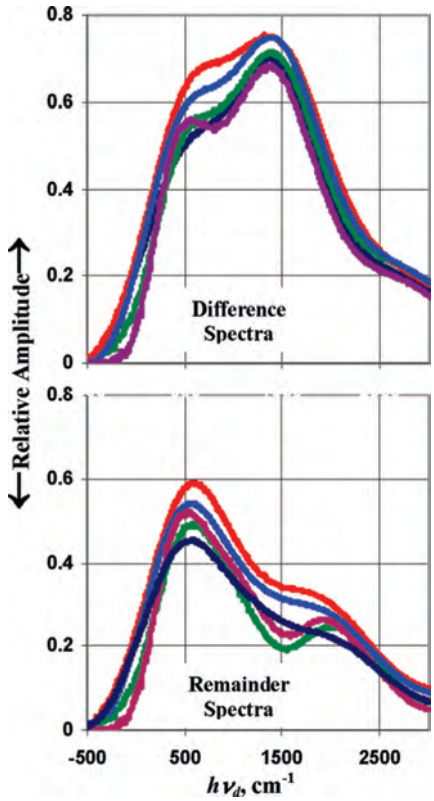

Figure 10. Difference (top panel) and remainder spectra (bottom panel) of $[Ru(Am)_{6-2n}(bpy)_n]^{2+}$ complexes.[26,27] $[Ru(NH_3)_4bpy]^{2+}$, blue; $[Ru(NH_3)_2(bpy)_2]^{2+}$, green; $[Ru(trien)bpy]^{2+}$, dark blue; $[Ru([14]aneN_4)bpy]^{2+}$, red; $[Ru(en)(bpy)_2]^{2+}$, plum. Amplitudes are relative to $I_{max(f)}$, and no corrections have been made for bandwidth variations.

contributions and that these are of very small amplitude in this region. The 3rd order contributions do account for a large percentage of the small amplitude emission intensities for $h\nu_d > \sim 2000$ cm^{-1} and we have only approximated these contributions, so the residuals in this region are intrinsically difficult to interpret.

It is significant that the combination of OB3 and *lf*1 models does lead to the maximum intensities for the envelopes of *lf* vibronic contributions in the range of 400−600 cm^{-1} for all of these complexes. This is as expected if these contributions arise largely from metal−ligand vibrational modes.

C. Modeled Band Shape of the $[Ru([12]aneN_4)bpy]^{2+}$ Complex. The fitting summarized in Table 1 assumes that the OB3 model provides a reasonable estimate of the bpy distortion mode vibronic contributions and that our deconvolution procedure overestimates the $I_{max(f)}$ for this complex; therefore, we have adjusted $I_{max(f)}$ by the minimum amount necessary so that $I_{\nu_d(diff)} \geq I_{\nu_d(OB3)}$ for all values of $h\nu_d$ (see Figure 11); the small negative value for ∂OB3 in the lower panel suggests that this underestimates the discrepancy in $I_{max(f)}$. The value of $R_{lf,mf} \geq 2.7$ found for this complex is by far the largest that we have found, and this is probably a lower limit since $h\nu_{max(lf)}$ is smaller than that found for any other complex so that there must be appreciable overlap with the fundamental component. These features make our estimate of $I_{\nu_m(f)}$ especially uncertain and the spectrum very difficult to fit.

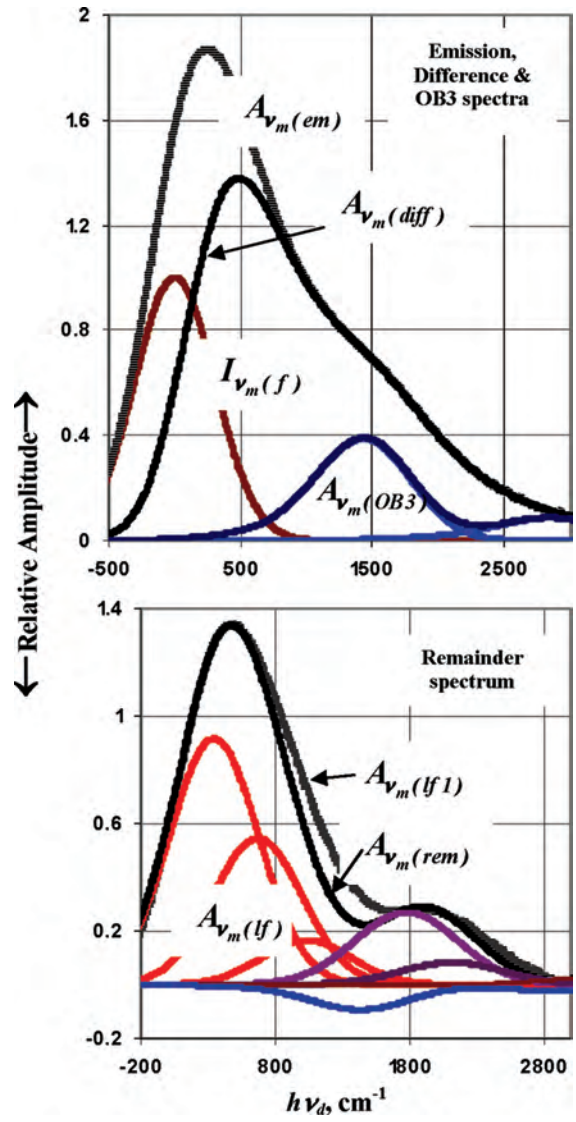

Figure 11. Emission, difference and OB3 spectra (top panel) and remainder spectrum (bottom panel) of $Ru([12]aneN_4)bpy]^{2+}$. The components are color coded as in Figure 7; the spectral amplitudes are adjusted so that $I_{\nu_d(diff)} \geq I_{\nu_d(OB3)}$ for all $h\nu_d$; $A_{\nu_m(OB3)}$ is based on $\Delta\nu_{1/2}$ of $I_{\nu_m(f)}$ and the attenuated (eq 12) $[Os(bpy)_3]^{2+}$[36] rR parameters; $I_{max(f)} = 1$.

D. $[Ru(py)_2(bpy)_2]^{2+}$ and $[Ru(py)_4bpy]^{2+}$ Complexes. These were also difficult complexes to model. The $[Ru(py)_4bpy]^{2+}$ complex is especially unusual in that $A_{3000(OB3)} \cong A_{3000(diff)}$ (see the red square in Figure 12). This behavior is similar to but not as extreme as that found for $[Ru([12]aneN_4)bpy]^{2+}$. Thus, this feature of the $[Ru(py)_4bpy]^{2+}$ spectral fit may similarly indicate appreciable overlap of the fundamental and *lf* vibronic components and a poor estimate of $I_{\nu_m(f)}$. Thus, the relatively smaller amplitude inferred in the spectral region corresponding to *lf*/OB3 combination band contributions ($h\nu_d \sim 2200$ cm^{-1}) for this complex suggests relatively smaller amplitude OB3 and/or *lf* vibronic contributions. Furthermore, the shape of the difference spectrum of $[Ru(py)_2(bpy)_2]^{2+}$ is poorly fit by a single equivalent *lf* vibronic component and suggests that at least two components are required to properly fit the *lf* region of this complex (Figure 12).[39]

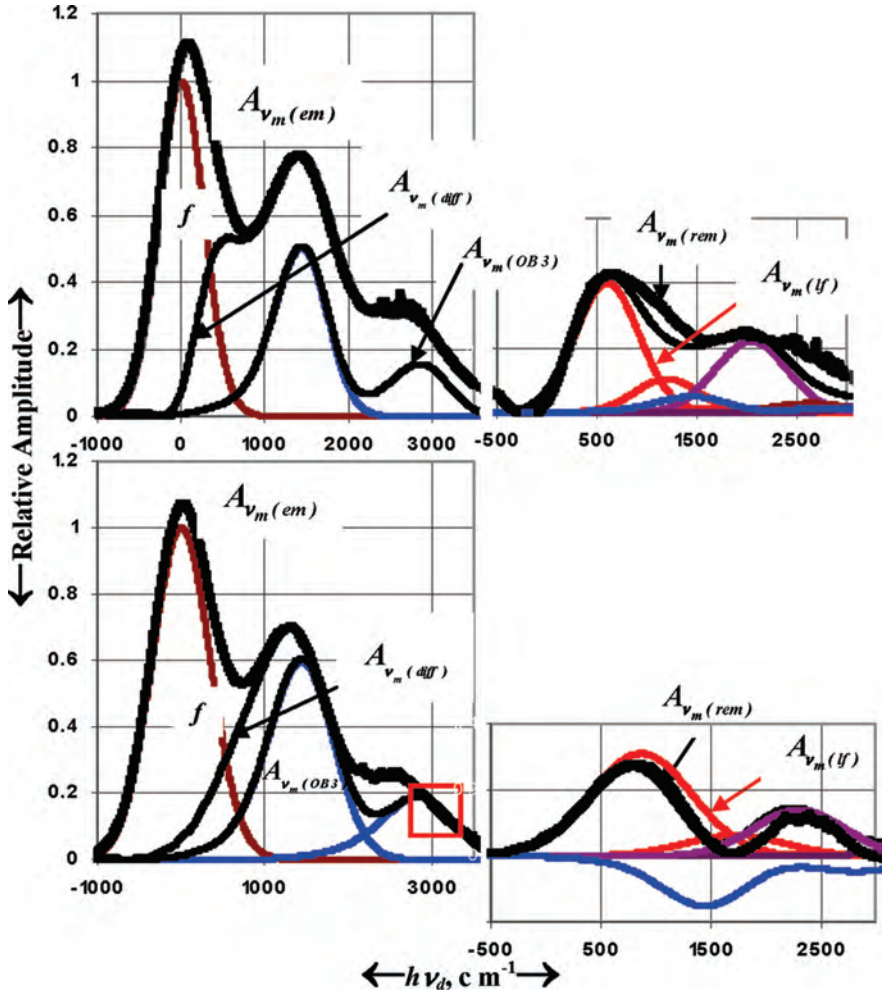

Figure 12. Comparison of the 77 K emission (left; thick black curves), difference (left; black curves), and remainder (right; thick black curves) spectra of $[Ru(py)_2(bpy)_2]^{2+}$, top panels, and $Ru(py)_4bpy]^{2+}$, bottom panels. For the panels on the left: the amplitude scales are relative to $I_{max(f)} = 1.00$ (dark red curve); and the abscissa for $h\nu_d = (h\nu_m - h\nu_{max(f)})$, cm^{-1}. The "progressions" in the *lf* component are color coded as in Figure 7.

E. $[Ru(CH_3CN)_n(X)_{2-n}(bpy)_2]^{n+}$ Complexes. The remainder spectrum of $[Ru(CH_3CN)_2(bpy)_2]^{2+}$ has a maximum at about 1900 cm^{-1} whose intensity is unusually large (~90% of the intensity of the *lf* maximum at 475 cm^{-1}). This feature is almost entirely attributable to the unusually large contribution of the *lf*/bpy combination band at $h\nu_d = h(\nu_{lf} + \nu_{bpy})$. The large intensity of this component arises because the MLCT excited-state energy is large enough that there is relatively little attenuation of the bpy distortion mode vibronic contributions while the maximum of the envelope of the *lf* contributions is comparable to or slightly larger than those found for the $[Ru(Am)_{6-2n}(bpy)_n]^{2+}$ complexes. This complex also has a significant (0.11) residual vibronic contribution at 1150 cm^{-1} and a substantial OB3 correction; see Supporting Information, Figure S14.[39]

The $[Ru(CH_3CN)(X)(bpy)_2]^+$ complexes (X = Cl or Br) were found to have relatively large values of $\Delta\nu_{1/2}$, and the envelopes of their *lf* vibronic contributions have maxima (545 and 640 cm^{-1}, respectively) at higher energies than one would expect for significant excited-state distortions in metal−ligand skeletal vibrational modes involving the Ru−X moieties. These features could be consequences of the convolution of such relatively *lf* vibronic components into the fundamental component that we evaluate from the emission spectrum.

F. $[Ru(X)_2(bpy)_2]$ Complexes. The *lf* vibronic contributions implicated by the difference and remainder spectra of these complexes are at relatively high energies, especially for X = NO_2, CN, and NCS in Figure 13. There is a very large range of vibronic amplitudes among these complexes.

1. X = Cl or Br. The preceding comments about the $[Ru(CH_3CN)(X)(bpy)_2]^+$ complexes are also applicable to these complexes (with some small differences in detail; see Supporting Information, Figure S15).[39]

2. X = NO_2. We were unable to obtain fits of the remainder spectrum of this complex that we can regard as satisfactory using the procedures described above (Figure 13). Because IL vibrational modes might be implicated if there were any LLCT/MLCT configurational mixing, we have also examined the possibility of two *lf* vibronic envelopes (see Supporting Information, Table S17;[39] NO_2^- vibrations are reported at about 550, 1185, and 1275 cm^{-1});[82] however, this introduces a new progression in some "equivalent" vibrational mode and requires some new set of

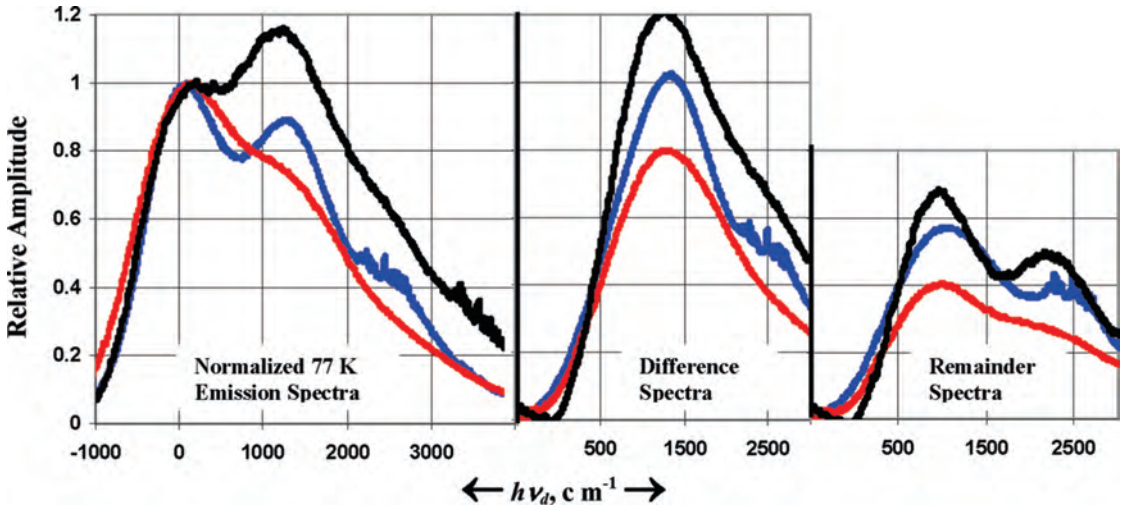

Figure 13. Comparison of the 77 K emission spectra (left), the difference spectra (middle), and the remainder spectra (right) of $[Ru(CN)_2(bpy)_2]$, blue; $[Ru((NO_2)_2(bpy)_2]$, black; and $[Ru(NCS)_2(bpy)_2]$, red. The intensity scales are defined so that $I_{max(f)} = 1.00$; $h\nu_d = (h\nu_m - h\nu_{max(f)})$, cm^{-1}. See also Supporting Information, Figure S16.[39]

assumptions about the appropriate combinations of modes that we are unable to test for these complexes, and the results of modeling with such an additional *lf* distortion mode were also not satisfactory.

3. X = CN. The OB3 and *lf*1 models fitted to the remainder spectrum of this complex also result in an equivalent "*lf*" vibronic contribution with an apparent value of $h\nu_{max(lf)}$ that is much larger than reasonable for the contributions arising from distortions in metal−ligand skeletal modes. In none of our fittings (see Supporting Information, Table S17)[39] did we find clear evidence for a vibronic contribution that could arise from the C≡N stretch.

4. X = NCS. The fundamental component has an even larger bandwidth for this complex, and the results are very similar to those described above for the cyano complex (see Figures 13 and Supporting Information, S16).[39] We found no clear evidence for any vibronic contribution that could be attributed to IL vibrational modes of the NCS^- ligand.

G. [Ru(R-carboxylato)(bpy)$_2$] Complexes. The emission spectra of the $[Ru(C_3H_2O_4)(bpy)]$, $[Ru(C_2O_4)(bpy)]$, and $[Ru(CO_3)(bpy)]$ complexes are similar as indicated in Figure 14, with the largest differences arising from the relatively small bandwidth and the larger amplitude *lf* vibronic component of the latter. The maximum of the *lf* vibronic envelope occurs for $h\nu_d > 550$ cm^{-1} for the dicarboxylates. While $h\nu_{max(lf)}$ appears to increase with $\Delta\nu_{1/2(lf)}$ for these complexes, the integrated amplitudes of their *lf* vibronic envelopes ($\approx 1.02A_{max(lf)} \times \Delta\nu_{1/2(lf)}$) differ by ≤7%.

H. X-ray Crystal Structure of [Ru(CH$_3$CN)(Cl)-(bpy)$_2$]$^{2+}$. Bond lengths and bond angles of the Ru coordination sphere for this structure (Figure 15) are presented in Table 3. The remaining structural details can be found in Supporting Information, S4 and at the Cambridge Crystallographic Data Centre.[39] The Ru−N≡C angle is 170° consistent with a small energy of the corresponding rocking vibrational mode. Thus, in solution one expects a distribution of Ru−N≡C conformers each with a slightly different solvation environment and a slightly different MLCT excited-state energy. Such distributions of conformers and/or solvates will contribute to the effective bandwidth and are probably a major reason for the relatively large bandwidths observed for the complexes with acetonitrile (and several other) ligands.

Discussion

A very wide range of 77 K Ru/bpy ^{3}MLCT excited-state emission bandshapes has been found for the $[Ru(L)_4bpy]^{m+}$ complexes. The spectator $(L)_4$ ligands of these complexes can be approximately grouped into classes (or combinations of classes) such as pyridyl, am(m)ine, halide, carboxalate, and so forth, and the emission bandshapes of complexes with different classes of these ligands are usually very similar. Most of the variations in emission band shape are characterized by differences in the relative and/or absolute amplitudes of vibronic contributions that arise from distortions in *mf*, largely bpy-centered ($h\nu_{mf} > 1000$ cm^{-1} for A_{mf}), or *lf*, largely Ru-ligand ($h\nu_{lf} < 1000$ cm^{-1} for A_{lf}), vibrational modes. Most of the variations in A_{mf}, and in distortions of bpy-centered vibrational modes, can be attributed to the differences in ground-state/MLCT configurational mixing that result when the excited-states energies differ, as discussed previously.[26,27,50] However, the variations in the relative amplitudes of A_{lf} and A_{mf} (or in the ratio of the first order *lf* and *mf* vibronic envelopes, $R_{lf,mf}$) are not readily related to simple electron transfer reorganizational parameters, and they most likely result from the configurational mixing of the ^{3}MLCT excited state with a higher energy metal-centered excited state (^{3}LF; see Supporting Information, S18).[39] Because emission bandshapes are correlated with excited-state structures, their variations implicate variations in excited-state reactivity.

A. Bandshape Modeling Issues. The rR[36,40,41] and 2 K doped single crystal[73] emission spectra of $[M(L)_4bpy]^{m+}$ complexes implicate MLCT excited-state distortions in more than 10 vibrational modes. Although these individual vibronic

(82) Drago, R. S. *Physical Methods for Chemists*; Harcourt Brace Jovanovich: Orlando, 1992.

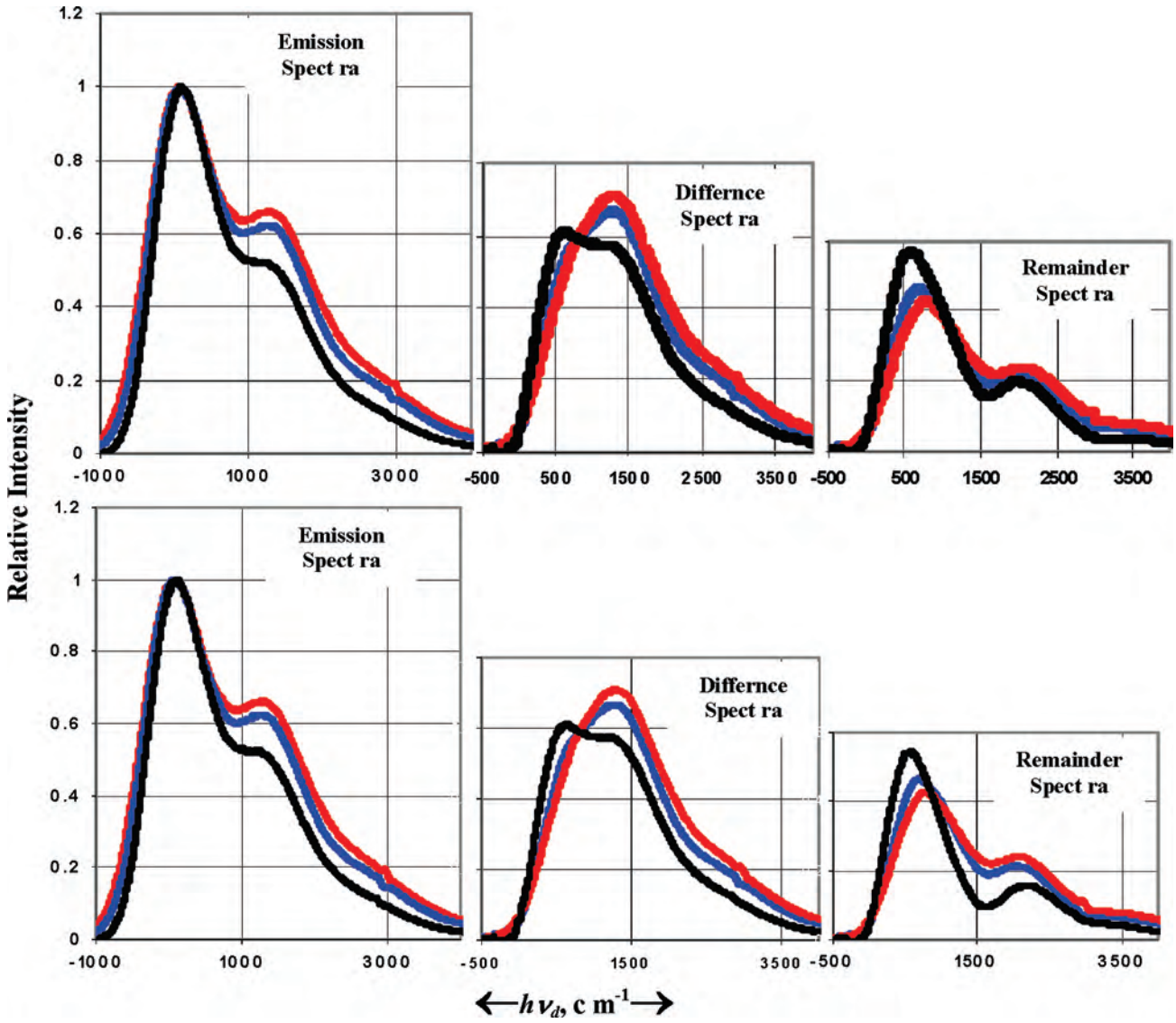

Figure 14. Comparison of the 77 K emission spectra (left panel), the difference spectra (middle panel), and the remainder spectra (right panel) of $[Ru(C_3H_3O_4)(bpy)_2]$, blue; $[Ru((CO_3)(bpy)_2]$, black; and $[Ru(C_2O_4)(bpy)_2]$, red. The intensity scales are defined so that $I_{max(f)} = 1.00$; $h\nu_d = (h\nu_m - h\nu_{max(f)})$.

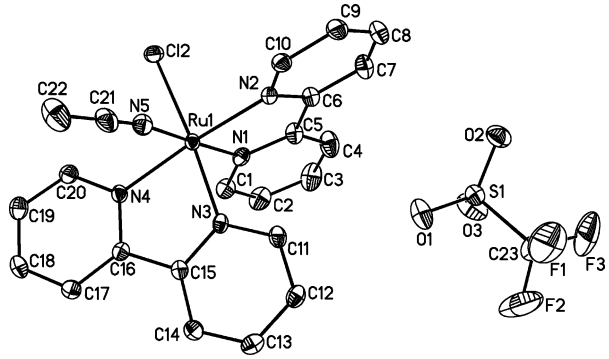

Figure 15. Molecular structure of $[Ru(CH_3CN)(CL)(bpy)_2][CF_3SO_3]$.

components are not resolved in the 77 K frozen solution spectra, structural information can still be obtained from the emission bandshapes of such spectra using a group frequency approach that is based on the envelopes of vibronic contributions in the spectral regions with vibrational frequencies that are characteristic of different functional groups within the

Table 3. Coordination Sphere Bond Lengths [A] and Angles [deg] for $[Ru(CH_3CN)(Cl)(bpy)_2][CF_3SO_3]$

bond or angle	Å or degrees	angle	degrees
Ru(1)−N(3)	2.0277(17)	N(2)−Ru(1)−N(4)	175.17(7)
Ru(1)−N(1)	2.0341(17)	N(3)−Ru(1)−Cl(2)	174.30(5)
Ru(1)−N(5)	2.0371(18)	N(1)−Ru(1)−Cl(2)	90.31(5)
Ru(1)−N(2)	2.0425(17)	N(5)−Ru(1)−Cl(2)	90.98(5)
Ru(1)−N(4)	2.0648(17)	N(2)−Ru(1)−Cl(2)	89.26(5)
Ru(1)−Cl(2)	2.4219(5)	N(4)−Ru(1)−Cl(2)	95.56(5)
N(3)−Ru(1)−N(1)	88.29(7)	C(1)−N(1)−Ru(1)	125.66(15)
N(3)−Ru(1)−N(5)	90.70(7)	C(5)−N(1)−Ru(1)	115.83(14)
N(1)−Ru(1)−N(5)	176.86(7)	C(10)−N(2)−Ru(1)	125.50(14)
N(3)−Ru(1)−N(2)	95.90(7)	C(6)−N(2)−Ru(1)	116.12(13)
N(1)−Ru(1)−N(2)	79.36(7)	C(11)−N(3)−Ru(1)	125.56(14)
N(5)−Ru(1)−N(2)	97.80(7)	C(15)−N(3)−Ru(1)	116.30(13)
N(3)−Ru(1)−N(4)	79.27(7)	C(20)−N(4)−Ru(1)	125.87(14)
N(1)−Ru(1)−N(4)	100.44(7)	C(16)−N(4)−Ru(1)	114.98(13)
N(5)−Ru(1)−N(4)	82.28(7)	C(21)−N(5)−Ru(1)	170.83(18)

complexes. The vibronic parameters inferred from the rR spectra of $[Os(bpy)_3]^{2+}$[36] and $[Ru(bpy)_3]^{2+}$[40] indicate that the contributions of metal−ligand vibronic modes to the excited-state distortions in the Os complex are only about

8% of those of the Ru complex (Figure 3), and this has led us to use the $[Os(bpy)_3]^{2+}$ rR parameters, allowing for the effects of variations in MLCT/ground-state configurational mixing, for an idealized estimate of the largely bpy-centered vibronic contributions in a two-center, (Ru^{III}/bpy) ^{3}MLCT excited state (the OB3 model). It is expected (and observed in rR spectra)[36,40,41] that the numbers, frequencies, and distortion amplitudes of these modes will vary from complex to complex. However, the variations in frequencies and relative component amplitudes are small in the *mf* regime, characteristic of bpy-centered vibrational modes when excited-state energies are similar (Figures 3 and Supporting Information, S7),[39] the *mf* envelopes constructed from the rR parameters reported for $[Os(bpy)_3]^{2+}$[36] and $[Ru(bpy)_3]^{2+}$[40] are very similar (Figure 3), and our observations on the $[Ru(L)_4bpy]^{m+}$ 77 K emission bandshapes indicate that the $[Os(bpy)_3]^{2+}$ rR parameters are very useful for modeling these contributions.

The principal remaining components in both the 77 K emission and the available rR spectra of the $[Ru(L)_4bpy]^{m+}$ complexes are the vibronic contributions of *lf*, largely Ru-ligand skeletal vibrational modes and their combination bands. These *lf* vibronic contributions appear to arise mostly from the configurational mixing between the ^{3}MLCT and a higher energy ^{3}LF excited state.[26–28] However, this raises some concerns about the generality of the correlation between vibronic parameters that are obtained from rR spectra and those contributing to the emission band shape since the energy differences between the LF and MLCT excited states is not likely to be the same in the singlet (probed by rR) and triplet (probed by emission) manifolds, and differences in these excited-state energies will result in differences in configurational mixing and in excited-state distortions in the singlet and triplet manifolds. Consequently, the rR-based and observed emission bandshapes may not always be the same.

We have used a fitting procedure in a single "equivalent" *lf* distortion mode (the *lf*1 model) that is based on modeling with the rR parameters reported[41] for $[Ru(NH_3)_4bpy]^{2+}$ to evaluate variations in the *lf* vibronic contributions in different complexes. The relative contributions of these *lf* components vary over a wide range (~3 fold) with variations of the "spectator" ligands suggesting a large range of ^{3}LF/^{3}MLCT configurational mixing in these complexes. On the other hand, the (*lf*1) model seems to be most generally applicable for $[Ru(Am)_4bpy]^{2+}$ complexes.

Our interpretations of emission bandshapes are based on a fundamental component,[37] $I_{\nu_m(f)}$, that is deconvoluted from the observed emission spectrum, and the Gaussian parameters from this component are used to determine the scale (ν_d) and amplitude for the experimental difference spectrum and the vibronic component bandwidths in the OB3 model. It has been demonstrated here and previously[26] that this fundamental component combined with rR parameters reproduces very well the 77 K emission bandshapes of the $[Ru(bpy)_3]^{2+}$ and $[Ru(NH_3)_4bpy]^{2+}$ complexes. This approach has given internally consistent and plausible results for "small" contributions from distortions in *lf* vibrational modes, $A_{max(lf)} < \sim 0.6$ and $h\nu_{max(lf)} \geq \sim 500$ cm^{-1}, and/or for relatively small component bandwidths, $\Delta\nu_{1/2} < \sim 1000$ cm^{-1}; for example, for all the $[Ru(Am)_{6-2n}(bpy)_n]^{2+}$ complexes except $[Ru([12]aneN_4)bpy]^{2+}$. Furthermore, the rR modeling indicates that it would be difficult to define meaningful *lf* and/or *mf* vibronic envelopes for $\Delta\nu_{1/2} < \sim 400$ cm^{-1} (see Figure 10 in Xie,[26] et al., and Supporting Information, S2[39]). That the largest deviations in our fits of the $[Ru(Am)_{6-2n}(bpy)_n]^{2+}$ complexes' difference spectra tend to be in the ranges of $\nu_d > \sim 2500$ cm^{-1} and $\nu_d \approx 1100-1300$ cm^{-1} is in remarkably good agreement with expectations since the former corresponds to the expected poor estimation of 3rd order vibronic contributions and the latter corresponds to vibronic contributions to the rR spectrum of $[Ru(bpy)_3]^{2+}$ but are not contained in the OB3 model. That the approach does not work well for complexes containing halide or pseudohalide ligands is most likely a consequence of a poor evaluation of $I_{\nu_m(f)}$, possibly as a consequence of unresolved overlap with very low energy vibronic components.

The group frequency approach in eq 2 seems to be a good basis for interpreting the general features of the observed band shape variations in series of closely related complexes. The OB3 part of this analysis should be useful guide for evaluating the band shape contributions of bpy-centered distortion modes to most metal-bpy MLCT emission spectra (note that the mixing coefficients, α_{ij}, in eq 12 will not generally be the same for Ru and other metal complexes), but the *lf*1 model is based on a fit to the rR parameters of $[Ru(NH_3)_4bpy]^{2+}$ and it may be less generally useful. Because this is an attempt to systematize the evaluation of ^{3}MLCT excited-state structures based on the contributions of different vibronic envelopes to the 77 K emission bandshapes of systems with a large number of distortion modes,[29–31,34–36,83,84] it can be anticipated that future studies and different techniques will provide better resolution of the key vibronic components, and thus a better characterization of the lowest energy MLCT excited states.

B. Some Implications of the Low Frequency Vibronic Contributions to the CT Emission Spectra of $[Ru(L)_4bpy]^{m+}$ Complexes. The appreciable $A_{\nu_m(lf)}$ emission band shape contributions found for the $[Ru(L)_4bpy]^{m+}$ complexes clearly demonstrate the inadequacy of single "equivalent" distortion mode models in describing the 77 K spectra, and more generally in developing structure−reactivity relationships for any series of Ru/bpy MLCT excited states. That $h\nu_{max(lf)} \approx 400-550$ cm^{-1} for the $[Ru(Am)_{6-2n}(bpy)_n]^{2+}$ and several other complexes is consistent with expectation for distortions in Ru−N coordination sphere vibrational modes. Because the amplitudes of these distortions are generally much larger than expected for simple Ru/bpy electron transfer (e.g., the ambient electron transfer properties of $[Ru(bpy)_3]^{2+}$ and $[Ru(NH_3)_4bpy]^{2+}$ imply that $\lambda_{lf} \sim 0$ and 80 cm^{-1}[21] and $A_{max(lf)} \sim 0$ and 0.16, respectively), the larger vibronic contributions found in the emission spectra most

(83) Single mode approaches have been used to fit emission spectra of these or related complexes,[29–31,34–36] and closely related two mode approaches have been reported recently in which it is assumed that $h\nu_{lf} = 400$ and $h\nu_{mf} = 1350$ cm^{-1}.[84]

(84) Abrahamsson, M.; Becker, H.-C.; Hammarstrolm, L.; Bonnefous, C.; Chamchoumis, C.; Thummel, R. P. *Inorg. Chem.* **2007**, *46*, 10354.

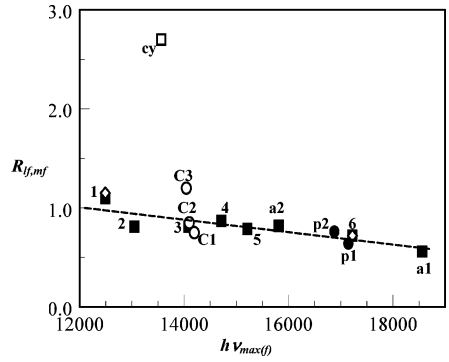

Figure 16. Correlation between the ratios of $R_{lf,mf}$ (ratio of low to *mf* vibronic contributions) and $E_{MLCT}{}^{0'0}$ in the 77 K emission spectra of $[Ru(L)_4bpy]^{m+}$ complexes. Complexes with $400 < \Delta\nu_{1/2}/cm^{-1} < 550$, solid squares: $(L)_4 = (NH_3)_4$, 1; trien, 2; [14]aneN$_4$, 3; $(NH_3)_2bpy$, 4; (en)bpy, 5; $(bpy)_2$, 6; $(CH_3CN)_2bpy$, a1; $(Cl^-)(CH_3CN)bpy$, a2. The other complexes are $(L)_4$ = [12]aneN$_4$)bpy, cy; $(C_2O_4{}^{2-})bpy$, c1; $(C_3H_2O_4{}^{2-})bpy$, c2; $(CO_3{}^{2-})bpy$, c3; $(py)_2(bpy)_2$, p1; $(py)_4bpy$, p2. The ratios represented as open diamonds were calculated from rR parameters (points 1 and 6).

likely arise from configurational mixing of the diabatic ^{3}MLCT excited states with somewhat higher energy, highly distorted ^{3}LF excited states. In the simplest limit, eq 2 suggests that $R_{lf,mf} = \int A_{lf}/\int A_{mf}$ is a function of the magnitude of LF/MLCT excited-state/excited-state configurational mixing where $\int A_{\gamma f} \approx 1.02 A_{max(xf)} \times \Delta\nu_{1/2(xf)}$ for Gaussian fits of the respective first order *lf* vibronic envelopes and the *mf* parameters based on the first order OB3 contribution. Thus, $\int A_{\gamma f} \approx \alpha_{LF,CT}{}^2 A_{LF}{}^{(d)}$ where $\alpha_{LF,CT} = H_{LF,CT}/\Delta E_{(LF,CT)}{}^{V''0'}$, $\Delta E_{(LF,CT)}{}^{V''0'}$ = the vertical energy difference between the LF excited state (V'' represents the vibrational quantum numbers in this LF excited state) and the MLCT excited state evaluated at the diabatic MLCT PE minimum, and $A_{LF}{}^{(d)}$ is a function of the Huang−Rhys parameters for the diabatic ^{3}LF excited-state or $A_{LF}{}^{(d)} \sim \sum_k S_k(LF)$. The attenuation effects that arise from MLCT/ground-state configurational mixing should approximately cancel in $R_{lf,mf}$, and there is only a little variation in $R_{lf,mf}$ for the $[Ru(Am)_{6-2n}(bpy)_n]^{2+}$ series of complexes ($R_{lf,mf(ave)} = 0.85 \pm 0.10$). However, there is a shallow decrease of this ratio with increasing $h\nu_{max(f)}$ (Figure 16) that could be consistent with a small, systematic decrease of the ^{3}LF excited-state PE minima,

$$\frac{A_{lf}}{A_{mf}} \cong 1.76 \pm 0.24 - (6.3 \pm 1.6) \times 10^{-5}\, h\nu_{max(f)} \quad (18)$$

That the values of $R_{lf,mf}$ for the [Ru(carboxylate)(bpy)$_2$] complexes (carboxylate = oxalate, malonate, and carbonate) are close to those predicted by eq 18 is consistent with their similar values of $E_{MLCT}{}^{0'0}$, the similarities of their coordinative environments, and the similarities of metal-N and metal-O vibrational frequencies. The observations for $[Ru(CH_3CN)_2(bpy)_2]^{2+}$, $[Ru(CH_3CN)(Cl)(bpy)_2]^+$, and $[Ru(py)_2(bpy)_2]^{2+}$ are also consistent with eq 18.

For $H_{LF,CT} \approx$ constant in the $[Ru(L)_4bpy]^{m+}$ complexes, the extent of LF/MLCT configurational mixing is a function of both the differences in the configurational coordinates of the two excited-state PE minima and the amplitudes of the ^{3}LF excited-state distortions; it is convenient to qualitatively represent the latter by $A_{LF}{}^{(d)}$ since this parameter is a function of the squares of displacements in the Ru-ligand vibrational modes. Thus, if $A_{LF}{}^{(d)}$ is approximately constant then eq 18 implies that the small changes in $\Delta E_{(LF,CT)}{}^{V''0'}$ in the series of complexes are the result of small decreases in differences of the PE minima, $\Delta E_{(LF,CT)}{}^{0''0'}$, of the two excited states as bpy ligands are replaced by am(m)ines, and this is more or less consistent with some of the ambient photochemical observations[85–89] and some DFT calculations.[90] However, the $[Ru(CH_3CN)_2(bpy)_2]^{2+}$ complex has a smaller value of A_{lf}, implying less configurational mixing, and a larger value of $\Delta E_{(LF,CT)}{}^{V''0'}$ than for any of the $[Ru(Am)_{6-2n}(bpy)_n]^{2+}$ complexes, yet the ambient photosubstitutional quantum yields are very large for this complex.[91] These observations can be reconciled if $A_{LF}{}^{(d)}$ is larger for $[Ru(CH_3CN)_2(bpy)_2]^{2+}$ than for the $[Ru(Am)_{6-2n}(bpy)_n]^{2+}$ complexes. Conversely, the markedly larger value of $R_{lf,mf}$ for [Ru([12]aneN$_4$)bpy]$^{2+}$ (see Figure 16 and Table 1) strongly suggests a less distorted ^{3}LF excited state since the coordinated [12]aneN$_4$ ligand is much less flexible than the other am(m)ine ligands considered here so that (a) the distortion of the Ru−N([12]aneN$_4$) bonds should be relatively small in the LF excited state; and (b) $\Delta E_{(LF,CT)}{}^{0''0'}$ should increase since the excited-state electron−electron repulsions will be greater for a small distortion of the metal ligand bond. These features require a relatively small value for $A_{LF}{}^{(d)}$ to be consistent with the very large value $R_{lf,mf}$ for the [12]aneN$_4$ complex in Figure 16.

When the distortions of ^{3}LF excited states of nd^6 metal centers are very large, as has been found for $[M(NH_3)_6]^{3+}$ complexes (see Supporting Information, S18),[39,45,46] there must be some set of distortions along metal−ligand nuclear coordinates Q'' for which the diabatic energy difference $\Delta E_{(LF,CT)}{}^{Q''0'}$ approaches zero, leading to a greatly distorted ^{3}MLCT excited-state PE surface near the resulting avoided crossing and analogous to the situation for mixed valence ground states.[15,92–94] If such distortions were to result in a double minimum for the adiabatic MLCT excited state, then a thermally promoted surface crossing could result in temperature dependent product yields without the population of higher energy excited states. Thus, the ammine ligands are likely to be more easily distorted than is bpy, and the extent of distortion could compensate for the changes in $E_{LF,CT}{}^{00'}$ through most of the $[Ru(Am)_{6-2n}(bpy)_n]^{2+}$ series. Furthermore, an adiabatic lowest energy excited-state PE surface with two local minima, such as might result from excited-state/excited-state configurational mixing combined with the presence of temperature dependent relaxation channels, could account for the complex temperature de-

(85) Malouf, G.; Ford, P. C. *J. Am. Chem. Soc.* **1977**, *99*, 7213.
(86) Ford, P. C. In *Inorganic and Organometallic Photochemistry*; Wrighton, M. S., Ed.; Amer. Chem. Soc.: Washington, DC, 1978; Vol. *168*, p 73.
(87) Maruszewski, K.; Stromen, D. P.; Kincaid, J. R. *J. Am. Chem. Soc.* **1993**, *115*, 8345.
(88) Maruszewski, K.; Kincaid, J. R. *Inorg. Chem.* **1995**, *34*, 2002.
(89) Sykora, M.; Kincaid, J. R. *Inorg. Chem.* **1995**, *34*, 5852.
(90) Alary, F.; Heully, J.-L.; Bijeireand, L.; Vicendo, P. *Inorg. Chem.* **2007**, *46*, 3154.
(91) Pinnick, D. V.; Durham, B. *Inorg. Chem.* **1984**, *23*, 3842.
(92) Hush, N. S. *Electrochim. Acta* **1968**, *13*, 1005.
(93) Hush, N. S. In *Mechanistic Aspects of Inorganic Reactions*; Rorabacher, D. B., Endicott, J. F. , Eds.; ACS Symposium Series 198; American Chemical Society: WA, 1982; p 301.
(94) Richardson, D. E.; Taube, H. *Coord. Chem. Rev.* **1984**, *60*, 107.

pendencies of the lifetimes and product quantum yields for complexes such as $[Ru(CH_3CN)_2(bpy)_2]^{2+}$ and $[Ru(py)_2(bpy)_2]^{2+}$.[91]

The MLCT excited-state distortions in *lf* vibrational modes, which our band shape analyses and the earlier resonance-Raman work have demonstrated to be characteristic of $[Ru(L)_4bpy]^{m+}$ MLCT excited states, are also relevant to nonradiative relaxation mechanisms of these complexes. Thus, when $h\nu_k \leq 4k_BT$ there will be significant thermal population of the vibrational excited-state of this mode in the ^{3}MLCT state, thereby providing a temperature dependent nonradiative relaxation channel.[69] It is important to note that in a multimode system, the relaxation channels need not be dominated by the harmonics of a single vibrational mode, and the very large number of channels with different combinations of vibrational modes can overwhelm the expected[69] dominance of relaxation channels composed of high frequency vibrational modes when displacements in the latter are very small.[26,28] As a consequence, distortions in *lf* modes might give rise to temperature dependencies of the excited-state lifetimes even without any contribution from the thermal population of higher energy excited states. It is clear that the effects of configurational mixings between electronic excited states and of the excited-state distortions near the forbidden crossings with the ground states of this class of complexes need to be clarified before their excited-state electron transfer properties can be considered to be understood or optimized for useful purposes.

Conclusions

In this report, we have developed a systematic approach for the analysis of the 77 K emission bandshapes of M-bpy complexes based on the hypothesis that the functional groups within these coordination complexes (bpy, metal−ligand, "spectator" ligand, etc.) have characteristic sets of vibrational modes and that the coupling between the vibrational modes of different functional groups is small, as is qualitatively expressed in eq 2. This approach provides a relatively straightforward means for probing the patterns of distortions in MLCT excited states, and thereby it can provide a systematic guide to patterns of excited-state reactivity.

Acknowledgment. The authors thank the Office of Basic Energy Sciences of the Department of Energy and the Office of the Vice President for Research of Wayne State University for partial support of this research.

Supporting Information Available: Tables of resonance-Raman parameters; issues of bandwidths and the relative of fundamental and vibronic component amplitudes; details of syntheses; structural parameters; absorption spectra of complexes; summary of electrochemical data; differences between Huang−Rhys parameters for $[Ru(bpy)_3]^{2+}$ and $[Os(bpy)_3]^{2+}$; OB3 model; systematic errors emission bandshapes when a single mode approximation is used for a multimode system; table of systematic evaluation of (*lf*1 + OB3) fits; summary of the possible bandwidth dependence of rR-based uncertainties in *lf*1 parameters; some details for fits of $[Ru(NH_3)_4bpy]^{2+}$ and $[Ru(bpy)_3]^{2+}$; polynomial fit of 3rd order vibronic contributions; electronic excited-state symmetries for $[Ru(bpy)_3]^{2+}$; modeled vibronic components of $[Ru(X)_2(bpy)_2]$ complexes; modeled vibronic components of $[Ru(CH_3CN)_n(X)_{2-n}(bpy)_2]$ complexes; fitting parameters for envelope of *lf* vibronic contributions to the emission spectra of $[Ru(NO_2)_2(bpy)_2]$ and $[Ru(CN)_2(bpy)_2]$ obtained for different input assumptions; ^{3}LF excited-state distortions. This material is available free of charge via the Internet at http://pubs.acs.org. Crystallographic data (without structure factors) for the structures reported in this paper have been deposited with the Cambridge Crystallographic Data Centre as supplementary publication no. CCDC-696319. Copies of the data can be obtained free of charge from the CCDC (12 Union Road, Cambridge CB2 1EZ, U.K.; tel: (+44) 1223−336−408; fax: (+44) 1223−336−003; e-mail: deposit@ccdc.cam.ac.uk).

IC7024473